Marine Heatwave Dynamics in James Bay: A Numerical Modelling Approach

By

Hannah Louisa Louis

A thesis submitted in partial fulfillment of the requirements for the degree of

Master of Science

Department of Earth and Atmospheric Sciences

University of Alberta

Abstract

The Hudson Bay and James Bay are critically understudied regions of the Arctic undergoing many changes due to climate change and Arctic Amplification. Cree and Inuit communities surrounding the bay have reported drastic changes in the marine environment since the late 1990s [1]. This thesis explores the connection that Marine Heatwaves (MHWs) may have played into these reported changes. With climate change and the associated increasing atmospheric temperatures and warmer, more open oceans, we will likely see more extreme MHWs. Therefore, identifying key drivers in MHW dynamics is important for understanding how southern Hudson Bay and James Bay (SHBJB) may be impacted in the future due to climate change. This thesis first explores how SHBJB sea surface temperature (SST) has responded over the past 21 years using the forced ocean model, Nucleus for European Modelling of the Ocean (NEMO). Then, the processes affecting MHWs are analysed using the model, calculating both the oceanic horizontal advection and the air-sea heat fluxes. To understand the dynamics further, two case studies with the highest SST anomalies are analysed closer, looking at both the years 2005 and 2017. These case studies follow a similar analysis, calculating both the horizontal advection and air-sea heat fluxes, and show that the shortwave and longwave radiative fluxes are the main driver that onsets the MHW event both years. Horizontal advection seems to play a secondary role in MHWs, either acting to prolong the event until ice cover begins to start, or creating another MHW event in the late fall/early winter. Lastly, this thesis explores sensitivity experiments that deviate from

the baseline experiment used for the initial MHW analysis. An extended time period with different atmospheric forcing is used as the first sensitivity experiment, showing MHWs that seem to match up with the same reports from local Indigenous communities of drastic climate change in the region. The final sensitivity experiment explore how added river temperatures affect the MHW dynamics in the SHBJB region, ultimately showing a null result.

Acknowledgements

First off, I want to thank my supervisor, Dr. Paul Myers. Thank you for all your support, mentorship, and giving me the opportunity to discover how amazing the ocean is. I also want give credit to you for making the Myers lab an awesome place to work— your enthusiasm for science and modelling is infectious.

To my fellow lab members: Tahya, Pouneh, Rowan, Ana, Robin, Mukulika, Adam, Andrew, Enrico, and Inge, thank you for making the lab a fun place to work as well as being awesome conference buddies to travel with.

To Laura Gillard: thank you for being such an amazing mentor and teacher in my undergrad, and for giving me the inspiration and courage to apply for grad school to continue learning about how awesome our world is.

Thank you to my dad, who taught me at a young age that education is so important and to always aspire to keep learning. Thank you to my mom for always supporting me and reminding me to never forget our culture and ceremony, even when things are really tough.

Finally, thank you to Jemma. I'm so grateful for you and all of your support, all of your help with trying to get the right words out, and for always being there for me when I get home to so we can just chill out and be goofy.

Contents

1 Introduction to Hudson Bay and James Bay: Geography, Climate, and People **1**

1.1 The Hudson Bay Complex Circulation 2

1.2 Climate Change in the North 6

1.3 Marine Heatwaves 7

1.4 In the Name of Scientific Inquiry 11

2 Methods **19**

2.1 Ocean Model 19

2.1.1 Model Equations and Assumptions 19

2.1.2 The Primitive Equations 21

2.1.3 Boundary Conditions 22

2.1.4 Grids and Discretization 23

2.1.5 Air-Sea Heat Flux Calculations 26

2.2 Sea Ice Model 28

2.3 Experimental Setup 29

2.3.1 Datasets 29

2.3.2 Model Evaluation 31

3 Results **41**

3.1 Methods 42

3.2 Data 44

3.3 Marine Heatwaves in James Bay, Canada 45

3.3.1 SST Analysis 46

3.3.2 Horizontal Advection 47

3.3.3 Air-Sea Heat Fluxes 49

3.4 Case Studies 50

3.4.1 2005 MHW 52

3.4.2 2017 MHW 57

3.5 Overview 58

3.6 Sensitivity Experiments 60

3.6.1 Air-Sea Forcing 61

3.6.2 River Heat 67

3.7 Summary 70

4 Conclusions **71**

4.1 Key Findings 71

4.1.1 Radiative heat fluxes are a primary driver for high SST anomaly years, with advection being a secondary driver to prolong events 71

4.1.2 Longer atmospheric forcing experiments capture MHW events reported by Indigenous communities, but have unexplained cold bias in recent years 72

4.1.3 Added river heat not significant in SHBJB region for MHW events . 72

4.2 Limitations and Future Work 73

List of Figures

1.1 The HBC and surrounding Cree and Inuit communities. Together, there are 38 Indigenous communities (25 Inuit communities and 13 Cree communities) [2]. In orange arrows is the general direction of surface current (adapted from [2]). 3

1.2 Seasonal pattern of Hudson Bay surface circulation [10]. 4

1.3 Different marine heatwave drivers visualized from the temperature tendency of the top mixed layer of the ocean [20]. 9

2.1 The Arakawa C-grid configuration from [31]. Located at the center are scalar variables temperature, salinity, pressure, and density. Vector points (u,v,w) are located at the grid faces and the vorticity points f, where the Coriolis force is defined, are located at the edges. Adapted from [31]. 26

2.2 ANHA4 model and AMSR2 satellite winter averaged (JFMA) sea ice concentration time series presented for the years AMSR2 data is provided (2013-2022). AMSR2 data was regridded to the ANHA4 grid using a bilinear method so direct comparison can be made. The calculated Pearson's correlation coefficient for the whole time series is r=0.97. 32

2.3 R/V William Kennedy observation locations for August 2021. Measurements were taken with a CTD instrument and over the course of 6 days from August 4 to August 9, 2023. Model points are taken from the nearest 5-day averages to encompass August 4 through 9. The 5-day averages thus chosen are model days August 3, 2021 and August 8, 2021, where the naming day is the middle day in the 5-day average. 33

2.4 Temperature vs Salinity (TS) diagram for August 2021 CTD observations from the R/V William Kennedy. The isopycnals (lines of constant density in kg/m^3 are shown in dashed lines). The red shaded squares are the nearest model points to the observations, which are shown as blue-green circles. The shading for both model and observations gets darker with depth. An outlier point can be seen at T=5°C and S=15 psu. This is likely an instrument error, but was chosen to be included in the plot. 34

3.1 Southern Hudson Bay and James Bay analysis region with depth contoured on top. The orange line indicates the transect at the "mouth" of James Bay in which all transports are calculated across. 45

3.2 SST anomaly in degrees Celsius in SHBJB for model run EPM151 for year 2002 to the end of 2022. MHW signatures can be seen in 2005, 2011, 2017, for example, with anomaly values of approximately 2.7, 3, and 3.3 degrees Celsius, respectively. Also shown in the plot are Marine Cold Spells (MCS), most noticeably in 2004 and 2019, with values of -4.6 and -3.5 degrees Celsius, respectively. 46

3.3 EPM151 monthly regional (SHBJB) averages of horizontal advection in degrees Celsius per second in the mixed layer depth (MLD) from 2002-2022. Negative indicated advection into the region (James Bay), whereas positive indicates advection out of the region. 48

3.4 Heat transport (degrees Celsius times Sverdrup) at the mouth of James Bay for EPM151. Negative sign indicates (southward) transport into the bay, whereas positive indicates (northward) transport out of the bay. 48

3.5 EPM151 sea ice concentration— as a fraction of a grid cell— regionally averaged for SHBJB in full ice cover months (January, February, March and April), spanning 2002 to the end of 2022. 49

3.6 EPM151 turbulent sensible heat flux monthly regional averages calculated using the COREBULK formula (as discussed in the methods section) for years 2002 to the end of 2022. Units are Watts per meter squared. Negative signs indicate heat going from atmosphere to ocean, whereas positive signs indicate heat going from ocean to atmosphere. 50

3.7 EPM151 turbulent latent heat flux (W/m^2) monthly regional averages calculated using the COREBULK formula— as mentioned in the methods— for 2002 to 2022. Directionality is similar to turbulent sensible heat flux. 51

3.8 The monthly averages of shortwave, longwave, and total radiative heat fluxes (W/m^2) for EPM151 years 2002-2022. The purple solid line is the longwave radiation, the blue solid line is the shortwave radiation, and the dashed black line is the net radiation. 51

3.9 EPM151 2005 SST anomaly with units of degrees Celsius. The lower yellow solid line indicates the 90th percentile quantile difference— defined by equation 3.8— while the solid orange line on top indicates the second quantile. The shaded yellow region is the first category of MHW, with temperatures between the first and second MHW categories, $2\Delta T$-ΔT. 53

3.10 EPM151 horizontal advection (degrees Celsius per second) for 2005. Negative indicated advection into the region (James Bay), whereas positive indicates advection out of the region 54

3.11 EPM151 heat transport at the mouth of James Bay, with units of ^{o}C Sv. Negative indicated advection into the bay, whereas positive indicates advection out of the region. 54

3.12 EPM151 turbulent sensible heat flux with units of W/m^2 for 2005. Negative signs indicate heat flux from the atmosphere to the ocean, whereas positive signs indicate heat flux from ocean to atmosphere. 55

3.13 EPM151 turbulent latent heat flux with units of W/m^2 for 2005. The directionality is similar to that of previous figures. 56

3.14 EPM151 2005 radiative fluxes with units in W/m^2. The purple solid line is the longwave radiation, the blue solid line is the shortwave radiation, and the dashed black line is the net radiation. The directionality for radiative flux plots differ than previous plots. Here, positive indicates heat fluxes into the ocean— heating the ocean— and negative is heat fluxes to the atmosphere— cooling the ocean. 56

3.15 EPM151 2017 SST anomaly with units of degrees Celsius. The lower yellow solid line indicates the first percentile quantile, while the solid orange line on top indicates the second quantile. The shaded yellow region is the first category of MHW, with temperatures between the first and second quantile. 57

3.16 Horizontal advection for 2017 58

3.17 EPM151 turbulent latent heat flux with units of W/m^2 for 2017. 59

3.18 EPM151 2017 radiative fluxes with units in Watts per meter squared. The purple solid line is the long wave radiation, the blue solid line is the shortwave radiation, and the dashed black line is the net radiation. 59

3.19 EPM111 SST anomaly from 1958-2021 with units of ^{o}C. The SST baseline ranges from 1980-2010. MHW signatures are seen most notably in 1998, 2001, and 2005, with maximum values of 5.4^{o}C, 4.9^{o}C, and 4.2^{o}C, respectively. Pearson's correlation coefficient between the two datasets is r=0.99. 62

3.20 SHBJB regional monthly averaged surface air temperatures in ^{o}C from 2002-2009 for CORE2-IA (blue) and NCEP-R2 (orange) reanalysis data. 63

3.21 EPM111 monthly regional average of horizontal advection (degrees Celsius per second) in SHBJB. The directionality is the same as figure 3.3 for EPM151. . 63

3.22 Heat transport (degrees Celsius times Sverdrup) at the opening of James Bay for EPM111. Directionality is the same as figure 3.4 for EPM151 64

3.23 EPM111 sea ice concentration— as a fraction of a grid cell— regionally averaged for SHBJB in full ice cover months (January, February, March and April), spanning 1958 to the end of 2021. 64

3.24 EPM111 monthly regional averages of turbulent sensible heat flux with units W/m^2 for years 1958 to 2021. 65

3.25 EPM111 monthly regional averages of turbulent latent heat flux with units W/m^2 for years 1958 to 2021. 65

3.26 EPM111 monthly averages of shortwave, long wave, and net radiative heat flux in W/m^2 for years 1958-2021. The purple solid line is the long wave radiation, the blue solid line is the shortwave radiation, and the dashed black line is the net radiation. 66

3.27 ETW161 SST anomaly in degrees Celsius from 2002-2018. MHW signatures are seen in years 2005, 2011, and 2017, with values above 2.5 degrees Celsius for the first two listed years, and over 3 degrees Celsius for 2017. 68

3.28 EPM151 (solid blue) and ETW161 (dashed orange) SST anomalies in ^oC contrasted together. 68

3.29 The SST anomaly difference between EPM151 and ETW161 in ^oC. The largest variations between the two experiments range only about 0.25^oC. 69

Chapter 1

Introduction to Hudson Bay and James Bay: Geography, Climate, and People

The Greater Hudson Bay Complex (HBC) is comprised of 5 main sub-regions— James Bay, Hudson Bay, Foxe Basin, Hudson Strait, and Ungava Bay. This encompasses 1.3 million km^2— equivalent to almost a fourth of the total surface area of Canada's surrounding oceans and Great Lakes [2]— and serves as one of the largest ocean drainage basins for freshwater in Canada with its watershed extending as far as the Alberta Rocky Mountains [3].

The focus of this study will be on southern Hudson Bay and James Bay (SHBJB). SHBJB is a seasonally ice covered inland sea with intense stratification due to immense freshwater input from the watershed. In general, this region behaves as a large estuary where the upper layer has a low salinity flux towards Hudson Strait balanced by an inward flux of higher salinity ocean water in the lower layer [4]. Due to the large presence of surface freshwater, either from river runoff or sea ice melt that spreads across the bay, there is little mixing

between the fresh and saline layers and thus was considered "dynamically dead" below 50m by early scientists studying Hudson Bay [2]. The SHBJB region is relatively shallow, with an average depth of 125m in Hudson Bay and 28.5m in James Bay [5]. The deepest part of James Bay is slightly over 100m, however, most of James Bay does not exceed 50m depth. In general, the bathymetry on the western side of James Bay is relatively gentle and the eastern side is more rugged [5].

Compared to other marine regions at similar latitudes, Hudson Bay and James Bay is colder due to the influx of cold Arctic waters and sea ice cover [2]. Breakup starts in the northwest and east coasts of Hudson Bay, where a large open-water polynya forms due to the prevailing north-westerly winds and persists throughout the ice cover season. Eventually, the breakup progresses towards the center of Hudson Bay where sea ice will be completely melted by July or August [2]. A vast majority of this sea ice is mobile, leading to ridging and thicker sea ice on the eastern side of the Bay. Sea ice in this region serves three very important functions: it provides a freshwater source via sea ice melt; serves as a habitat for wildlife such as polar bears and seals; and, it provides a ground for surrounding Indigenous communities to travel and hunt [2].

Although sparsely populated, this region is the homeland of many Cree and Inuit communities (figure 1.1) whose way of life is heavily intertwined with this environment. The Inuit of this region are known as "people of the sea ice" whereas the Crees have extensive knowledge of freshwater and coastal environments which extends hundreds of kilometers inland from the coast [2].

1.1 The Hudson Bay Complex Circulation

The HBC serves as a detour where cold, fresh arctic water cycles through before heading to the Labrador Sea and the North Atlantic. Buoyant freshwater from the arctic will make its

Figure 1.1: The HBC and surrounding Cree and Inuit communities. Together, there are 38 Indigenous communities (25 Inuit communities and 13 Cree communities) [2]. In orange arrows is the general direction of surface current (adapted from [2]).

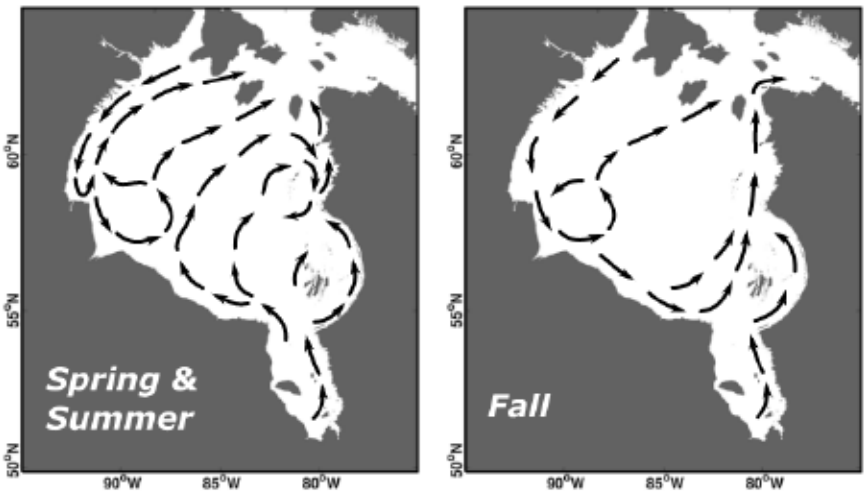

Figure 1.2: Seasonal pattern of Hudson Bay surface circulation [10].

way through the Canadian Arctic Archipelago, most of which will flow through Baffin Bay southwards to the Labrador Sea [4]. Relatively small amounts of arctic freshwater will end up flowing southward through Fury and Hecla Strait and end in the HBC system starting off in Foxe Basin [4][2][6]. Although a relatively small amount of arctic water takes this pathway, it is dramatically changed throughout its journey. Foxe Basin has some of the worlds strongest tides. Here, the arctic water will undergo tidal mixing and transform into vertically mixed, homogeneous water [4]. After Foxe Basin, water will flow south into Hudson Bay either through Roes Welcome Sound— located between mainland Nunavut in the northwest and Southampton Island, where Coral Harbour in figure 1.1— or northern Hudson Strait [2][7][8].

Being one of Canada's largest drainage basins, the HBC receives about 900 km^3/year of river runoff, which is approximately a quarter of the total river runoff input into the Arctic Ocean [9]. The freshwater input from rivers induces a geostrophic boundary current in Hudson Bay and James Bay [10][5]. Cree and Inuit communities recognize that the tidal phase and the 500+ rivers that input into the HBC are important drivers of the currents [7]. As states by Inuit Elder, Noah Isaac, "When the high tide and strong currents come, it is time to look for beluga whales because the winds will be strong and coming from the northwest [...] That is when you expect to see beluga at the floe edge" [7].

Shown in figure 1.1 is the Hudson Bay coastal cyclonic (counter-clockwise) circulation that is driven by geostrophic winds and buoyancy from freshwater input [2][4][10]. A more in depth understanding of the circulation of James Bay is lacking— few studies have been done to quantify this. Of the studies investigating this, most were spurred on by the hydroelectric development of La Grande River to quantify the pre-development circulation [5]. A limitation of these early studies was that they were based off of summer survey data, as winter in-situ data was difficult to obtain due to ice cover. Classifying James Bay as following an estuarine circulation model, Prinsenberg used a theoretical model to understand the circulation [5]. This theoretical model involves calculating seven base equations: conservation of salt, temperature, mass, the three equations of motion, and the equation of state.

Prinsenberg calculated surface current drift values using data in available months for James Bay and found that the pre-hydroelectric development circulation behaves similar to a fjord estuarine circulation at the entrance of the bay. This behaviour changes further south into the bay and behaves as a partially-mixed estuary; incoming surface water from southern Hudson Bay is relatively fresh due to river input but distinguishable from water in James Bay due to more input of river water [5]. This cold, relatively salty water circulates from Hudson Bay into western James Bay, and eventually leaves through eastern James Bay into Hudson Bay as a narrow tongue of warm, low-salinity water due to deflection to the right via the Coriolis force [5]. Both western and eastern water masses are separated from the deep water by a sharp pycnocline. However, due to the shallower shelf in western James Bay and greater tidal mixing, the pycnocline is weaker on the west side [5].

Normally in Hudson Bay, strong cyclonic geostrophic currents occur on the coasts with little exchange with the weaker flows of the interior. In more recent studies, Ridenour et al. shows that summer mean circulation can be modified from the general circulation pattern to include small pockets of both cyclonic and anti-cyclonic circulation throughout the bay (figure 1.2) [10]. The salinity changes due to springtime river runoff freshet and sea ice melt causes the

sea surface height to be higher in the east than the west. These changes in steric height gradients pushes water westward and then deflects right into the center of Hudson Bay due to the Coriolis force, thus directing the circulation up through the middle of the bay [10]. The wind stress curl and Ekman transport also contributes to the reversal of the cyclonic flow. Here, the surface stress curl becomes negative at the start of spring and stays that way until the fall. The atmosphere also plays a role— Ekman transport is shown to accumulate seawater and increase the sea height in southeastern Hudson Bay.

After the circulation is makes its way throughout Hudson Bay and James Bay, water will flow northward and out through the south side of Hudson Straight cyclonically through Ungava Bay [6][8], eventually ending up in northern Labrador Sea where it will make its way south in the Labrador Current.

1.2 Climate Change in the North

The climate is rapidly changing in northern regions. An emerging trend is arising globally: Indigenous people are disproportionally affected by climate change despite having little negative impact on their environments. This is especially true for Indigenous people in Canada's North. Adding to this injustice is the lack of climate services in the North, where uncertainty remains high in remote areas for seasonal forecasts and long-term projections. This is especially dangerous in this region, where travel and hunting grounds is provided by sea ice and there is high risk and uncertainty associated with ice thinning.

Starting in the late 1990s, the Cree and Inuit communities surrounding Hudson Bay and James Bay began to notice and report drastic changes in the climate, which to this day is rapidly changing the local environment. Some local impacts include dramatic decline in eelgrass meadows, warmer and shorter winters, and erratic and unpredictable weather and sea ice patterns. According to community members, "It is now impossible to predict our

weather; our ancient methods of forecasting weather are no longer yielding the predicted patterns." [7].

According to the Hudson Bay Integrated Regional Impact Study (IRIS) [2], we can expect to see a multitude of ocean changes in the Greater Hudson Bay Marine Region. With increased sea ice melt in the polar region, sea level rise will start to erode the Manitoba and Ontario coastlines in western Hudson Bay [11]. However, the rate of increase of sea level rise is less than the rate of isostatic rebound. That is, due to the removal of the weight of the last ice sheet, the land is rising at a faster rate than the sea level increase. This, however, does not mean that the HJB coasts will be "spared"; it is also predicted that the frequency of storm surges along eastern Hudson Bay and Hudson Strait will increase, leading to more treacherous conditions [2][11][12].

In terms of sea surface temperature (SST), the HBC is seeing a response to climate change largely linked to the shortening of the ice season. Galbraith & Larouche [13] show that there is a high correlation between the maximum SST in the summer and the amount of open water. Here, the date the ice break up finishes is more important than the onset of breakup in regards to high SST anomalies in the summer. Linking this to the future climate, model projections show that the increase in SST in polar regions is $\sim 2^{o}$. Lukovich et al. [14] used numerical ocean models to simulate the future impact of climate change on the Hudson Bay Complex over 1981-2070 based on an ensemble of climate scenarios. As expected, global warming results in increases in SST. However, for every emission scenario, the range of possible outcomes of SST increases the further the model simulates into the future.

1.3 Marine Heatwaves

Climate change is progressing much more rapidly in the Arctic compared to the rest of the world. Due to this "Arctic Amplification" [15], the North is warming nearly four times faster

than the global average [16]. Such warming can cause drastic changes in the environment including but not limited to multiyear sea ice loss [17] and longer ice-free seasons [13]. Sea ice loss can lead to positive feedback loops, where less sea ice leads to a lower albedo and more atmospheric heat uptake, thereby leading to warmer oceans and more sea ice loss [18], as well as more marine heatwaves (MHW) events in non-Arctic environments. These increasing atmospheric temperatures and warmer, more open oceans are exacerbating extreme anomalous warm water events known as marine heatwaves (MHW). According to the framework proposed by Hobday et al. [19], MHWs are defined to be a prolonged anomalous warming event where the temperature is sustained above a threshold— usually at least 5 days with temperatures consistently above the 90th percentile of the climatological average— with each MHW event being discrete and having clear start and end dates.

As with its atmospheric counterpart, MHWs have many complex physical processes that drive and influence the dynamics of these events. We can understand MHW dynamics— from formation to demise by breaking down each physical component of a mixed layer temperature budget [20]. The following formula is given by Moisan and Niiler [21] and describes the vertically averaged temperature tendency of water in the mixed layer [20].

$$\begin{aligned}\frac{\partial \overline{T}}{\partial t} = &-\overline{\mathbf{u}} \cdot \nabla \overline{T} \; + \; \overline{\nabla \cdot (\kappa_h \nabla T)} \; - \; \frac{1}{h} \kappa_z \frac{\partial T}{\partial z}\bigg|_{-h} \\ &- \left(\frac{\overline{T} - T_{-h}}{h}\right)\left(\frac{\partial h}{\partial t} \; + \; \mathbf{u}_{-h} \cdot \nabla h \; + \; w_{-h}\right) \\ &+ \frac{Q_{SW} \; + \; Q_{SW(-h)} \; + \; Q_{LW} \; + \; Q_{sens} \; + \; Q_{lat}}{\rho c_p h}\end{aligned} \tag{1.1}$$

In this equation, $\overline{T}$ is the temperature of the mixed layer, $\mathbf{u}$ is the two-dimensional horizontal ocean velocity, w is the vertical velocity, h is the depth of the mixed layer, κ_h and κ_z are the horizontal and vertical diffusivity coefficients, and ρ and c_p are the density and specific heat capacity of seawater, respectively. Q encompasses each different term for the air-sea heat flux: Q_{SW} is the shortwave radiative flux, $Q_{SW(-h)}$ is the shortwave radiative flux leaving the

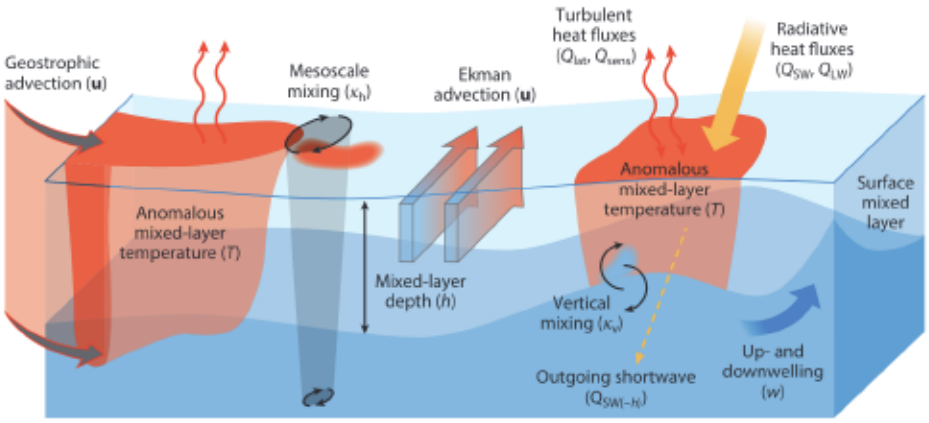

Figure 1.3: Different marine heatwave drivers visualized from the temperature tendency of the top mixed layer of the ocean [20].

bottom of the mixed layer, Q_{LW} is the longwave radiative flux, Q_{sens} is the turbulent sensible heat flux, and Q_{lat} is the turbulent latent heat flux. This equation describes how different physical processes, such as horizontal advection, air-sea heat flux, and vertical mixing, affect the rate of change of temperature in the mixed layer via the transfer of heat [20].

The process that dominates the MHW event is said to be the primary driver, whereas the process that contributes second is called the secondary process [18]. Higher-order contributing processes are tertiary and are generally neglected in analysis. The two most dominant processes that drive MHWs tend to be horizontal advection and air-sea heat flux. Anomalous ocean currents or anomalous temperature gradients are responsible for advective-type MHWs [20]. Air-sea heat flux can be due to numerous processes. For example, weaker winds can decrease the latent heat loss from ocean to air—Q_{lat} flux going from ocean to atmosphere decreases— subsequently increasing ocean temperatures. Also, sensible heat loss from ocean to air can decrease when surface air temperatures are warm. In terms of radiative heat transfer to the ocean, less cloud cover can lead to greater amount of shortwave radiation reaching the ocean surface for absorption, thereby increasing sea surface temperatures (SST).

In the global ocean, Bian et al [22] investigate the role of mesoscale eddies— which account for approximately 70% of world ocean kinetic energy— and show that they play a crucial

role in driving mesoscale MHWs, especially in the initial onset or growing phase. Thus, it is important that ocean models can resolve mesoscale eddies. Similarily, Richaud et al [18] shows that horizontal advective heat fluxes act as the physical driver for onsetting most MWHs in the main Arctic gateway regions. Richaud et al [18] also brings up an important point when dealing with Arctic MHWs: Arctic wintertime conditions can be very stable with surface water temperatures at the freezing point for several months. Thus, the 90th percentile threshold can be very close to the climatological mean and a very small departure from the freezing point (of the order of a few hundredth of a Celsius degree) can lead to the detection of an MHW.

More and more frequently, coastlines around the world are experiencing days of extremely high SST, with Hudson Bay and James Bay seeing some of the highest and longest coastal warming in the past few decades [23]. With background SST continuing to rise over the next few decades, anthropogenic climate change is likely to dramatically increase the number of MHW events and eventually, it is expected that the global ocean will reach a permanent MHW state [20] [24]. This highlights the need for a moving baseline instead of a fixed baseline climatology.

These events can not only have lasting impacts on the local marine life, but in Hudson Bay and James Bay, MHWs can affect the surrounding Cree and Inuit communities whose way of life rely heavily on their connection to the Arctic marine environment. Many studies on MHW are motivated by the impacts they have on ecological life. Different regions will have different species, tolerances, and rates of adaptation. How tolerant and well-adjusting key species in SHBJB— for example, eel grass or beluga whales— is unknown. This further motivates regional studies on MHWs.

1.4 In the Name of Scientific Inquiry

Despite the research done previously, there is still a lot that is unknown about the southern Hudson Bay and James Bay. For example, possible outcomes in model simulations begin to diverge the farther out into the future is simulated, with SST increases ranging from 1^{o}C to 3^{o}C in the HBC [14]. Not only this, but climate change is accelerating the uncertainties in HBC's environmental conditions: adverse weather and unpredicted sea ice melt are rendering local traditional navigational knowledge as unreliable [2][7]. The lack of observational data (apart from traditional knowledge) and overall climate services in the HBC compounds this danger. Thus, the future of the Hudson Bay is largely uncertain. For example, a loss in sea ice would not only impact the local transport routes, but it would also be a detriment to the Indigenous communities in the region, as they rely on key marine species such as beluga whales or seals as a major food source. As mentioned previously, local Indigenous people reported abrupt change in the marine environment in SHBJB starting in the late 1990s. Coinciding with this change is a MHW event in 1998 in James Bay, followed by other extreme MHWs the following two decades. Firstly, this research aims to answer the following question: Are MHWs responsible for the drastic changes seen in the region? Based on the rising occurrences of MHW in coastal regions, it is hypothesized that MHWs are in part responsible for the reported oceanic regime change in SHBJB. If this is so, it will be critical to determine the processes that are important drivers for MHWs in SHBJB. Figuring out the MHW dynamics in SHBJB will be important in future studies looking at forecasted scenarios and future impacts in the region.

This thesis will focus on answering these questions. First, an overview of the methods used will be given. This includes an overview of the numerical ocean model, Nucleus for European Modelling of the Ocean (NEMO), as well as the coupled sea-ice model, Louvian-la-Nueve sea ice model version 2 (LIM2). Then, a description of the model experiments used will be given as well as a discussion on relevant datasets and model evaluation. Next, results from

an analysis on MHWs in SHBJB will be provided, including air-sea heat flux and horizontal advection calculations. Finally, we will conclude and discuss the results of the MHW and what the implications are for these results.

Bibliography

[1] Nunavut Cambridge Bay. "Elder's Conference on Climate Change". In: (2001).

[2] ZA Kuzyk and LM Candlish. "From science to policy in the greater Hudson Bay marine region: An integrated regional impact study (IRIS) of climate change and modernization". In: *ArcticNet, Québec City* (2019), p. 424.

[3] Environment Canada and Climate Change. *Government of Canada*. Nov. 2017. URL: https://www.canada.ca/en/environment-climate-change/services/freshwater-quality-monitoring/hudson-bay-watershed.html.

[4] RG Ingram and S Prinsenberg. "Coastal oceanography of Hudson Bay and surrounding eastern Canadian Arctic waters". In: *The sea* 11.29 (1998), pp. 835–859.

[5] Simon J Prinsenberg. *Analytical study of the circulation of James Bay*. Fisheries and Environment Canada, 1978.

[6] Ran Tao and Paul G Myers. "Modelling the advection of pollutants in the Hudson Bay complex". In: *Journal of Marine Systems* 214 (2021), p. 103474.

[7] Miriam Anne McDonald, Lucassie Arragutainaq, and Zacharassie Novalinga. "Voices from the Bay: Traditional ecological knowledge of Inuit and Cree in the Hudson Bay bioregion". In: *(No Title)* (1997).

[8] Natasha A Ridenour et al. "Hudson Strait inflow: Structure and variability". In: *Journal of Geophysical Research: Oceans* 126.9 (2021), e2020JC017089.

[9] Igor A Shiklomanov and Alexander I Shiklomanov. "Climatic change and the dynamics of river runoff into the Arctic Ocean". In: *Water Resources* 30 (2003), pp. 593–601.

[10] Natasha A Ridenour et al. "Revisiting the circulation of Hudson Bay: Evidence for a seasonal pattern". In: *Geophysical Research Letters* 46.7 (2019), pp. 3891–3899.

[11] CD Smith et al. "CanCoast: A national-scale framework for characterizing Canada's marine coasts". In: *11th International Symposium for GIS and Computer Cartography for Coastal Zone Management*. 2013.

[12] A-M Hayden et al. "Multi-Century Impacts of Ice Sheet Retreat on Sea Level and Ocean Tides in Hudson Bay". In: *Journal of Geophysical Research: Oceans* 125.11 (2020), e2019JC015104.

[13] Peter S Galbraith and Pierre Larouche. "Reprint of "Sea-surface temperature in Hudson Bay and Hudson Strait in relation to air temperature and ice cover breakup, 1985–2009"". In: *Journal of Marine Systems* 88.3 (2011), pp. 463–475.

[14] Jennifer V Lukovich et al. "Simulated impacts of relative climate change and river discharge regulation on sea ice and oceanographic conditions in the Hudson Bay Complex". In: *Elem Sci Anth* 9.1 (2021), p. 00127.

[15] Roman V Bekryaev, Igor V Polyakov, and Vladimir A Alexeev. "Role of polar amplification in long-term surface air temperature variations and modern Arctic warming". In: *Journal of Climate* 23.14 (2010), pp. 3888–3906.

[16] Mika Rantanen et al. "The Arctic has warmed nearly four times faster than the globe since 1979". In: *Communications Earth & Environment* 3.1 (2022), p. 168.

[17] Walter N Meier and Julienne Stroeve. "An updated assessment of the changing Arctic sea ice cover". In: *Oceanography* 35.3/4 (2022), pp. 10–19.

[18] Benjamin Richaud et al. "Drivers of marine heatwaves in the Arctic Ocean". In: *Journal of Geophysical Research: Oceans* 129.2 (2024), e2023JC020324.

[19] Alistair J Hobday et al. "A hierarchical approach to defining marine heatwaves". In: *Progress in oceanography* 141 (2016), pp. 227–238.

[20] Eric CJ Oliver et al. "Marine heatwaves". In: *Annual review of marine science* 13 (2021), pp. 313–342.

[21] John R Moisan and Pearn P Niiler. "The seasonal heat budget of the North Pacific: Net heat flux and heat storage rates (1950–1990)". In: *Journal of Physical Oceanography* 28.3 (1998), pp. 401–421.

[22] Ce Bian et al. "Oceanic mesoscale eddies as crucial drivers of global marine heatwaves". In: *Nature communications* 14.1 (2023), p. 2970.

[23] Fernando P Lima and David S Wethey. "Three decades of high-resolution coastal sea surface temperatures reveal more than warming". In: *Nature communications* 3.1 (2012), p. 704.

[24] Eric CJ Oliver. "Mean warming not variability drives marine heatwave trends". In: *Climate Dynamics* 53.3 (2019), pp. 1653–1659.

[25] Gurvan Madec et al. "Ocean general circulation model reference manual". In: *Note du Pôle de modélisation* (1997).

[26] Martin Vancoppenolle et al. "The Louvain-la-Neuve sea ice model". In: *Notes du pole de modélisation, Institut Pierre-Simon Laplace (IPSL), Paris, France* 31 (2012).

[27] JL Bamber et al. "Land ice freshwater budget of the Arctic and North Atlantic Oceans: 1. Data, methods, and results". In: *Journal of Geophysical Research: Oceans* 123.3 (2018), pp. 1827–1837.

[28] Fedor Mesinger and Akio Arakawa. "Numerical methods used in atmospheric models". In: (1976).

[29] Andre J Robert. "The integration of a low order spectral form of the primitive meteorological equations". In: *Journal of the Meteorological Society of Japan. Ser. II* 44.5 (1966), pp. 237–245.

[30] Richard Asselin. "Frequency filter for time integrations". In: *Monthly Weather Review* 100.6 (1972), pp. 487–490.

[31] Gurvan Madec et al. "NEMO ocean engine". In: (2017).

[32] William George Large and Stephen G Yeager. *Diurnal to decadal global forcing for ocean and sea-ice models: The data sets and flux climatologies*. 2004.

[33] Thierry Fichefet and MA Morales Maqueda. "Sensitivity of a global sea ice model to the treatment of ice thermodynamics and dynamics". In: *Journal of Geophysical Research: Oceans* 102.C6 (1997), pp. 12609–12646.

[34] Ralph Timmermann et al. "On the representation of high latitude processes in the ORCA-LIM global coupled sea ice–ocean model". In: *Ocean Modelling* 8.1-2 (2005), pp. 175–201.

[35] Sylvain Bouillon et al. "An elastic–viscous–plastic sea ice model formulated on Arakawa B and C grids". In: *Ocean Modelling* 27.3-4 (2009), pp. 174–184.

[36] WD Hibler III. "A dynamic thermodynamic sea ice model". In: *Journal of physical oceanography* 9.4 (1979), pp. 815–846.

[37] Elizabeth C Hunke and John K Dukowicz. "The elastic–viscous–plastic sea ice dynamics model in general orthogonal curvilinear coordinates on a sphere—Incorporation of metric terms". In: *Monthly Weather Review* 130.7 (2002), pp. 1848–1865.

[38] Laura C Gillard. "Modelling the Interconnection of the Ocean and the Greenland Ice Sheet". In: (2021).

[39] *Mercator Ocean*. `https://www.mercator-ocean.eu/en/ocean-science/glorys/`. Accessed: 2024-06-10.

[40] Michael Steele, Rebecca Morley, and Wendy Ermold. "PHC: A global ocean hydrography with a high-quality Arctic Ocean". In: *Journal of Climate* 14.9 (2001), pp. 2079–2087.

[41] Seiji Yukimoto et al. "A new global climate model of the Meteorological Research Institute: MRI-CGCM3—Model description and basic performance—". In: *Journal of the Meteorological Society of Japan. Ser. II* 90.0 (2012), pp. 23–64.

[42] A Dai. *Dai and Trenberth Global River Flow and Continental Discharge Dataset [Dataset].* Accessed: 2024-06-10. 2017. DOI: https://doi.org/10.5065/D6V69H1T.

[43] TA Stadnyk et al. *Hydrological modeling of freshwater discharge into Hudson Bay using HYPE. Elem. Sci. Anthr. 8.* 2020.

[44] Christiaan T van Dalum et al. "First results of the polar regional climate model RACMO2. 4". In: *EGUsphere* 2024 (2024), pp. 1–36.

[45] Gregory C Smith et al. "A new atmospheric dataset for forcing ice–ocean models: Evaluation of reforecasts using the Canadian global deterministic prediction system". In: *Quarterly Journal of the Royal Meteorological Society* 140.680 (2014), pp. 881–894.

[46] Tahya WeissGibbons et al. "Increased runoff from Siberian rivers leads to Arctic wide freshening". preprint available at https://essopenarchive.org/users/659901/articles/663686-increased-runoff-from-siberian-rivers-leads-to-arctic-wide-freshening.

[47] *Advanced Microwave Scanning Radiometer 2 (AMSR2).* https://www.earthdata.nasa.gov/learn/find-data/near-real-time/amsr2. Accessed: 2024-07-08.

[48] *Southern Hudson Bay - James Bay CTD Data 2021.* https://canwin-datahub.ad.umanitoba.ca/data/dataset/hudson-bay-james-bay-ctd-2021. Accessed: 2024-07-08.

[49] *Kiel Climate Model System.* https://www.geomar.de/kcms. Accessed: 2024-07-12.

[50] *WMO guidelines on the calculation of climate normals.* Doc. WMO-No. 1203, WMO, Geneva. 2017.

[51] Alistair J Hobday et al. "Categorizing and naming marine heatwaves". In: *Oceanography* 31.2 (2018), pp. 162–173.

[52] *NCEP/DOE Reanalysis II.* ttps://psl.noaa.gov/data/gridded/data.ncep.reanalysis2.tml. Accessed: 2024-06-42.

[53] Daqing Yang et al. "Heat flux, water temperature and discharge from 15 northern Canadian rivers draining to Arctic Ocean and Hudson Bay". In: *Global and Planetary Change* 204 (2021), p. 103577.

Chapter 2

Methods

2.1 Ocean Model

This thesis uses the Nucleus for European Modelling of the Ocean (NEMO) version 3.6 as its ocean modelling framework. This model has three components: for ocean dynamics and thermodynamics, NEMO uses Ocean PArallélisé (OPA) [25], a model that uses the primitive equations to study both regional and global ocean circulation; a coupled sea ice dynamics and thermodynamics model, Louvain La-Neuve Ice Model version 2 (LIM2) [26]; and Tracer in the Ocean Paradigm (TOP) to provide physical constraints for passive ocean tracers and biogeochemical processes. The ocean and sea ice model will be discussed in further detail below.

2.1.1 Model Equations and Assumptions

The NEMO model using a curvilinear coordinate system to solve the primitive equations that include the Navier-Stokes equations as well as a nonlinear equation of state which together can

couple temperature and salinity to the fluid velocity. The following are model assumptions made in consideration of scale:

Spherical earth approximation

The Earth is approximated to be a sphere, rather than an ellipsoid. Thus, the geopotential surfaces are spheres and therefore gravity is parallel to the radius of the Earth.

Thin-shell approximation

The depth of the ocean is much less than the radius of the Earth and is therefore negligible when considering the distance from the center of the Earth.

Turbulent closure hypothesis

The advection term in the Navier-Stokes equations— that is the change in momentum and buoyancy due to advection— is non-linear and encompasses the effects of turbulent motion. Turbulent fluxes occur on scales smaller than the grid resolution and is a relatively small part of the primitive equations; however, its influence on large scale dynamics is important due to its long term balance of the surface input of kinetic energy and heat. Therefore, turbulence is parameterized in order to close the system of equations by way of a turbulent closure scheme, like the Turbulent Kinetic Energy (TKE) closure scheme among others.

Boussinesq hypothesis

Variations in ocean density are small. Therefore, density variations are assumed constant and are neglected unless they contribute to the buoyancy force.

Hydrostatic hypothesis

The vertical momentum equation is simplified as the balance between the buoyancy force and vertical pressure gradient force. Convective processes are thus parameterized.

Incompressibility hypothesis

Seawater is treated as an incompressible fluid. Thus, the divergence of the three-dimensional velocity is zero.

2.1.2 The Primitive Equations

The primitive equations are as follows:

Conservation of Momentum

$$\frac{\partial \mathbf{U}_h}{\partial t} = -\left[(\nabla \times \mathbf{U}) \times \mathbf{U} + \frac{1}{2}\nabla(\mathbf{U}^2)\right]_h - f\mathbf{k} \times \mathbf{U}_h - \frac{1}{\rho_o}\nabla_h p + \mathbf{D}^{\mathbf{U}} + \mathbf{F}^{\mathbf{U}} \tag{2.1}$$

Hydrostatic Equilibrium

$$\frac{\partial p}{\partial z} = -\rho g \tag{2.2}$$

Incompressibility Equation

$$\nabla \cdot \mathbf{U} = 0 \tag{2.3}$$

Conservation of Heat

$$\frac{\partial T}{\partial t} = -\nabla \cdot (T\mathbf{U}) + D^T + F^T \tag{2.4}$$

Conservation of Salt

$$\frac{\partial S}{\partial t} = -\nabla \cdot (S\mathbf{U}) + D^S + F^S \tag{2.5}$$

Equation of State

$$\rho = \rho(T, S, p) \tag{2.6}$$

where $\mathbf{U}$ is the vector $(\mathbf{i}, \mathbf{j}, \mathbf{k})$ velocity, ρ_o is a reference density, $\frac{\partial}{\partial t}$ is the time derivative, ∇ is the vector derivative in the $(\mathbf{i}, \mathbf{j}, \mathbf{k})$ directions, t is time, z is the vertical coordinate, ρ is the in-situ fluid density, p is the pressure, g is the gravitational constant, T is potential temperature, S is salinity, h denotes the horizontal $(\mathbf{i}, \mathbf{j})$ vector, and the Coriolis acceleration is denoted by f=$2\mathbf{\Omega} \cdot \mathbf{k}$. Small-scale physics parameterizations are denoted by $\mathbf{D^U}, D^T, D^S$ for momentum, temperature, and salinity. Likewise, $\mathbf{F^U}, F^T, F^S$ are surface forcing terms. The equation of state (equation 2.1.2) solves for the seawater density, which depends on temperature, salinity, and pressure.

2.1.3 Boundary Conditions

Just like in reality, the ocean model must be constrained by boundaries. These boundaries include interfaces of the solid Earth-ocean, land-ocean, atmosphere-ocean, and sea ice-ocean. Some of these interaction are weak, even on longer time scales. For example, the solid earth-ocean boundary, heat and salt fluxes are usually so small, they are neglected in the model. However, for momentum, the solid boundary has a no-slip condition, meaning that velocity, and thus momentum, must be zero. Friction is also important for momentum fluxes at solid boundaries. These small-scale turbulent fluxes must be parameterized in the model (denoted by $\mathbf{D^U}$). The land-ocean boundary— where river runoff from the land is included— is especially important in high-latitude oceans. The Arctic Ocean is a beta-ocean, meaning that it is strongly stratified and governed by a halocline rather than a thermocline. Thus,

river runoff is an important interaction at this interface. Precipitation and evaporation— commonly denoted by PE (Precipitation minus Evaporation)— is another major source of freshwater flux the model must take into account. This occurs at the atmosphere-ocean boundary and is a dynamic boundary condition; precipitation is supplied by the atmospheric forcing product— it is not influenced by the ocean interaction— but evaporation dynamically links the atmosphere and ocean via the temperature and humidity gradients between the two realms. Glacial melt is also a source of freshwater flux, and it must be provided in the model, either from other models or from databases like Bamber18 (short for Bamber 2018) [27]. Heat flux is also provided at the atmosphere-ocean boundary as both long wave and shortwave radiation and dynamically links the two by latent and sensible heat fluxes. Freshwater and heat flux are also provided at the lateral boundaries. For ANHA4, these quantities are can be provided from different sources, such as global reanalysis data or a globally run ocean model. Lastly, the sea ice-ocean boundary is an important source for heat, salt, and freshwater flux due to the very low salinity sea ice melt-freeze cycle ($\sim$4 psu compared to $\sim$34 psu for the ocean), as well as drag for momentum exchange between the ice and ocean.

2.1.4 Grids and Discretization

Eulerian models must be discretized in space and time in order to calculate the governing equations. For the horizontal grid, many ocean models choose to use Arakawa C-grid [28] where scalar variables like temperature, salinity, pressure, and density are located and solved at the grid center and velocity vector components are located on the grid faces (see figure 2.1). The C-grid can come up with a computational mode due to the offset of the u- and v-grids, however many models still choose to use it, as opposed to a B-grid, in which case the model would have a double average of the pressure gradient term.

Global and regional Arctic ocean models also face an interesting problem at the North Pole. Here, a singularity occurs when the latitude and longitude lines converge. To bypass this

numerical issue, models can use different grid types to eliminate the North Pole singularity. Grid solutions include using an irregular grid, unstructured grid, or tri-polar grid. Irregular grids may use finite elements, such as triangles, that can be adjusted in their size and resolution. The downside to this method is that it is computationally expensive, and it can cause issues with advection on geostrophic scales and spurious diapycnal mixing. Unstructured or adaptive grids change dynamically with time, but are computationally expensive and are not as developed as other grid methods. Tri-polar grids are what NEMO uses, which is much more computationally efficient and is set up with the singularities occurring on land (in Northern Canada and Siberia). The NEMO horizontal ocean mesh is created with a tri-polar grid and a curvilinear coordinate system where each cell dimension locally deformed by the scale factors (e_1, e_2, e_3). These are defined as the following:

$$e_1 = R\left[\left(\frac{\partial\lambda}{\partial i}\cos\phi\right)^2 + \left(\frac{\partial\phi}{\partial i}\right)^2\right] \tag{2.7}$$

$$e_2 = R\left[\left(\frac{\partial\lambda}{\partial j}\cos\phi\right)^2 + \left(\frac{\partial\phi}{\partial j}\right)^2\right] \tag{2.8}$$

$$e_3 = \left(\frac{\partial z}{\partial k}\right) \tag{2.9}$$

where i, j, k indicate the direction or spatial dimension, the Earth's radius, R, is simplified from (R+z) due to the thin-shell approximation, and λ and ϕ being the longitude and latitude, respectively.

Three main vertical coordinate systems are used for numerical ocean models, each with their own advantages and disadvantages. The most common is the z-coordinate system, which is based on the number of depth levels and usually has the thinnest and highest concentration of

levels nearest to the surface. Terrain-following or σ-coordinates are exactly how they sound— they mimic the bathymetry and they are based on the fraction of ocean depth scaled between 0 and 1. Finally, there are density coordinates, which are defined based on the isopycnals.

The continuous governing equations listed previously must also be discretized in time. The NEMO model uses the following three-level time scheme for time discretization:

$$x^{t+\Delta t} = x^{t-\Delta t} + 2\Delta t \ \mathrm{RHS}_{x}^{t-\Delta t, t, t+\Delta t} \tag{2.10}$$

where x is either T, S, u, or v, Δt is the time step, and RHS is the right hand side of the time evolution equation, and the superscript is the time step the quantity is solved at. For non-diffusive processes— momentum, advection, pressure gradients, and Coriolis terms— NEMO uses the so-called leap frog method of time integration, where the RHS is evaluated at time step 1 (i.e., it is time-centered). This second-order accuracy method does not artificially damp out linear oscillatory motion or cause instability by amplify these oscillations. This method does not represent diffusion nor Rayleigh damping and it is associated with large phase speed errors. To mitigate this, NEMO uses the Robert-Asselin [29][30] time filter and either forward- or backward schemes are used for diffusive processes.

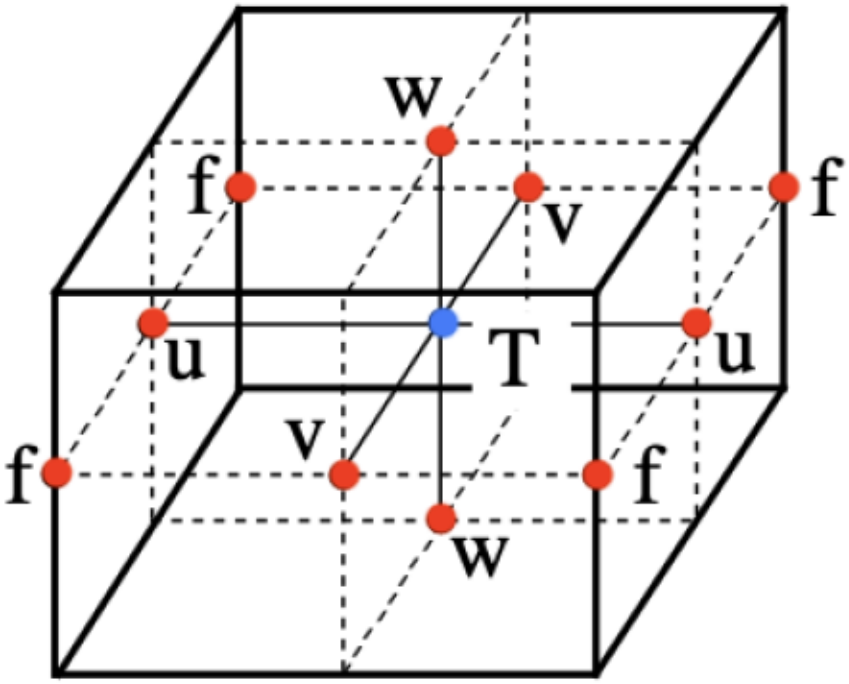

Figure 2.1: The Arakawa C-grid configuration from [31]. Located at the center are scalar variables temperature, salinity, pressure, and density. Vector points (u,v,w) are located at the grid faces and the vorticity points f, where the Coriolis force is defined, are located at the edges. Adapted from [31].

2.1.5 Air-Sea Heat Flux Calculations

The net air-sea heat flux is given by the following:

$$Q_{net} = Q_{sw} + Q_{lw} + Q_{sens} + Q_{lat} \tag{2.11}$$

where Q_{sw} is the heat flux from incoming shortwave radiation, Q_{lw} is from the longwave radiation, Q_{sens} is the sensible heat flux, and Q_{lat} is the latent heat flux. The shortwave radiation flux is provided solely by the atmospheric forcing product. The NEMO model has

different turbulent heat flux formulations built in. In this thesis, all model experiments use the COREBULK formula [32] to calculate turbulent fluxes. This formula describes the exchange of heat between atmosphere and ocean depending on their temperatures, humidity, velocities, and drag coefficients. Below is the COREBULK formulation, with ice concentration taken out into account.

$$Evap = \rho_a C_E \left(q(z_q) - q_{sat}(SST)\right) |\Delta \mathbf{U}| \tag{2.12}$$

$$Q_{lat} = L_v \times Evap \tag{2.13}$$

$$Q_{sens} = \rho_a c_p C_H \left(\theta(z_\theta) - SST\right) |\Delta \mathbf{U}| \tag{2.14}$$

where ρ_a is the density of air near the surface ($\rho_a = 1.22 kg/m^3$), C_E is the transfer coefficient for evaporation, C_H is the transfer coefficient for sensible heat, $q(z_q)$ is the specific humidity at z height (where z is some height in meters), $|\Delta \mathbf{U}|$ is the wind modulus, L_v is the latent heat of vaporization, $\theta(z_\theta)$ is the potential air temperature, c_p is the specific heat capacity, q_{sat} is the specific humidity of saturated air given by the following formula:

$$q_{sat}(q_1, q_2, SST) = \rho_a^{-1} \left(0.98 \times 640380 \frac{kg}{m^3}\right) e^{\frac{-5107.4K}{SST}} \tag{2.15}$$

where coefficients q_1 is equal to $0.98 \times 640380 \frac{kg}{m^3}$ and q_2 is equal to $-5107.4K$. The long wave heat flux is given by the non-solar heat flux, i.e., the long wave radiation coming from the atmosphere, clouds, etc., minus the blackbody radiation emitted by the ocean, given by the Stefan-Boltzmann law.

$$Q_{lw} = Q_{lw}^{atmos} - \sigma T^4 \tag{2.16}$$

where the Stefan-Boltzmann constant $\sigma = 5.67 \times 10^{-8} \frac{W}{m^2 K^4}$.

2.2 Sea Ice Model

Hudson Bay is a seasonally ice covered inland sea. Thus, the model requires the use a sea ice model coupled with the ocean model. All model experiments in this thesis use the dynamic-thermodynamic Louvain la Nouveau sea ice model version 2 (LIM2) [33][34]. The two-dimensional dynamic component of this model is influenced by both the atmosphere and ocean via the conservation of linear momentum of ice:

$$m\frac{\partial \mathbf{u}}{\partial t} = \nabla \cdot \bar{\bar{\sigma}} + A\left(\tau_a + \tau_w\right) - mf\hat{k} \times \mathbf{u} + mg\nabla\eta \tag{2.17}$$

where m is the ice mass per unit area, u is the horizontal ice velocity, $\bar{\bar{\sigma}}$ is the internal ice stress tensor, A is the ice area fraction, τ_a and τ_w are the respective wind and ocean stress, f is the Coriolis parameter, g is gravitational acceleration, and η is the ocean surface height [35]. Therefore, the sea ice momentum is dependent on wind and ocean stress, sea surface height, and sea ice internal stress. Calculating the internal stress tensor involves calculating the viscous-plastic (VP) formulation, originally developed by Hibler [36]. However, a faster method developed by Hunke and Dukowicz [37] called the elastic-viscous-plastic (EVP) is used in LIM2 to calculate the internal stresses [35].

The sea ice thermodynamic component of LIM2 includes a three-level model— with one snow layer and two ice layers—to determine the vertical and horizontal growth and decay

[33][34][35]. The internal temperatures of snow and ice are given by the one-dimensional vertical heat conduction equation:

$$\rho c_p \frac{\partial T}{\partial t} = G_h k \frac{\partial^2 T}{\partial z^2} \tag{2.18}$$

where ρ is the ice or snow density, c_p is the specific heat capacity, k is the thermal conductivity, G_h is a correction factor to account for variations in heat conduction due to variation in unresolved ice thicknesses[33][38]. The thermodynamic component also calculates the surface growth and decay using a heat balance with incoming radiative fluxes, turbulent fluxes, and conductive heat flux from the bottom.

2.3 Experimental Setup

This thesis uses model experiments ANHA4-EPM151, ANHA4-EPM111, and ANHA4-ETW161. EPM151 serves as the baseline experiment in which the other two will be compared to as sensitivity experiments in chapter 3. As indicated by the name, all use model resolution $\frac{1}{4}^o$ with the ANHA domain. Additionally, all relevant model experiments include tides, have a 5-day average output, and are coupled to the LIM2 ice module. Table 3.1 provides information on the model experimental setup, including forcing, initial conditions, and significant characterizations.

2.3.1 Datasets

Atmospheric forcing data is provided by the Canadian Meteorological Centre Global Deterministic Prediction System ReForecasts (CGRF), derived from the global deterministic prediction system (GDPS). This is reforecast data, as opposed to reanalysis, meaning that it

Experiment	Integration	IC	BC.	Atmospheric Forcing	Runoff
EPM151	2002-2022	GLORYS2v3	GLORYS2v3	CGRF	A-HYPE/B18
EPM111	1958-2022	PHC3.0	Kiel_K3415	CORE-IA	DT/B18
ETW161	2002-2018	GLORYS2v4	GLORYS2v4	CGRF	A-HYPE/B18

Table 2.1: Model runs used in this thesis and their setup. Column 3 lists the configuration initial conditions, where GLOYS2v3 come from the Mercator Ocean Team [39] and PHC comes from the Polar Science Center [40]. Column 4 lists the Boundary conditions, where Kiel comes from Geomar climate model and MRI comes from the Meteorological Research Institute's General Climate Model (CGM) [41]. For runoff DT is the Dai and Trenberth [42], B18 is Bamber [27] Greenland runoff., and A-HYPE is the Arctic implementation of the HYdrological Predictions for the Environment (HYPE) hydrological model [43] and RACMO is from the Regional Atmospheric Climate Model [44]

.

is simply operational forecasts from the GDPS model [45]. Other atmospheric forcing datasets for hindcasts include reanalysis data from the coordinated ocean-ice reference experiments version 2 (CORE-IA). For initial conditions and boundary conditions in EPM151— as well as for ETW161— GLORYS $\frac{1}{4}^o$ reanalysis from Mercator Ocean is used. Here, ocean model output is combined with existing observations to synthesize an estimate of the state of the ocean. For EPM111, boundary conditions are derived from Geomar's Kiel eOCRA025 ocean model, based on NEMO. Initial conditions for EPM111 use Polar Science Center Hydrographic Climatology (PHC), which merges the World Ocean Atlas observational data with data from the Arctic Ocean Atlas, thus creating a more comprehensive global climatology with better representation of the Arctic Ocean [40].

For EPM111, runoff is provided by Dai and Trenberth [42] which has monthly river runoff data from 925 of the worlds largest rivers as well as continental discharge rates, but fails to include any interannual variability after 2007. For these experiments, Greenland runoff is provided separately by Bamber 2018 [27] which is derived from a combination of climate model, satellite, and terrestrial data. For EPM151 and ETW161, river runoff is provided by the A-HYPE hydrological model, developed specifically for the Arctic and Hudson Bay drainage system. However, A-HYPE still uses Dai and Trenberth outside the Arctic and Hudson Bay drainage systems. River heat is included with the discharge in ETW-161, pro-

viding a more realistic model representation than previous experiments, which inputs river discharge at the same temperature as the ocean near the river mouth [46] [in review]. All experiments use Bamber 2018 [27] for Greenland runoff.

For sea ice concentration, model results are compared to satellite data from the Advanced Microwave Scanning Radiometer 2 (AMSR2) datasets [47]. This data is regridded from the 6.25km National Snow and Ice Data Center (NSIDC) North Polar Stereographic grid to the ANHA4 grid for direct comparison. For temperature and salinity data comparison, TS plots are compared with CDT data from the Research Vessel William Kennedy James Bay 2021 cruise [48].

2.3.2 Model Evaluation

The ability for numerical models to accurately represent real physical processes must be considered given that models represent large and complex systems, thus model drift and can occur and through deficiencies in forcing, setup, resolution, etc., the model may also poorly represent observed features. Model evaluation is typical and offers a way to quantitatively determine how "close to reality" our model is, either by comparing model output to observational data, or in some cases where observations are sparse, an ensemble of other models. For the southern Hudson Bay and James Bay (SHBJB) region, model evaluation in this thesis is provided for sea ice concentration, as well as temperature and salinity.

For sea ice, the model is evaluated with ice concentration comparing it to AMSR2 data. The model well represents ice concentration in the SHBJB region for the main ice cover seasons (January through April) with high confidence. This is shown in figure 2.2, which has a Pearson's correlation coefficient of r=0.97 for the time series.

Model temperature and salinity (TS) can also be evaluated with observations from CTD (Conductivity-Temperature-Depth) instruments. In August 2021, the Research Vessel William

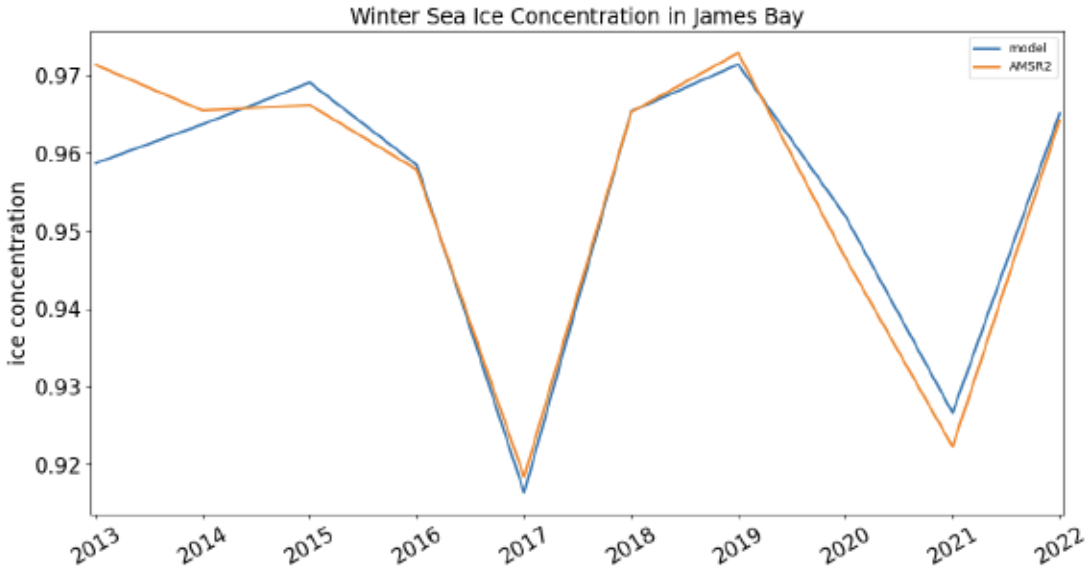

Figure 2.2: ANHA4 model and AMSR2 satellite winter averaged (JFMA) sea ice concentration time series presented for the years AMSR2 data is provided (2013-2022). AMSR2 data was regridded to the ANHA4 grid using a bilinear method so direct comparison can be made. The calculated Pearson's correlation coefficient for the whole time series is r=0.97.

Kennedy sailed throughout James Bay and recorded periodic CTD measurements at locations shown in figure 2.3. To compare to the model, the nearest model days and model points where taken and TS diagrams were plotted (figure 2.4). It can be seen that while the model TS captures the general spread of the observed TS at depth, what is missing is the freshness of water likely coming from river runoff. This model experiment (EPM151) also does not include river temperature, which likely also explains the lack of the warmer surface water.

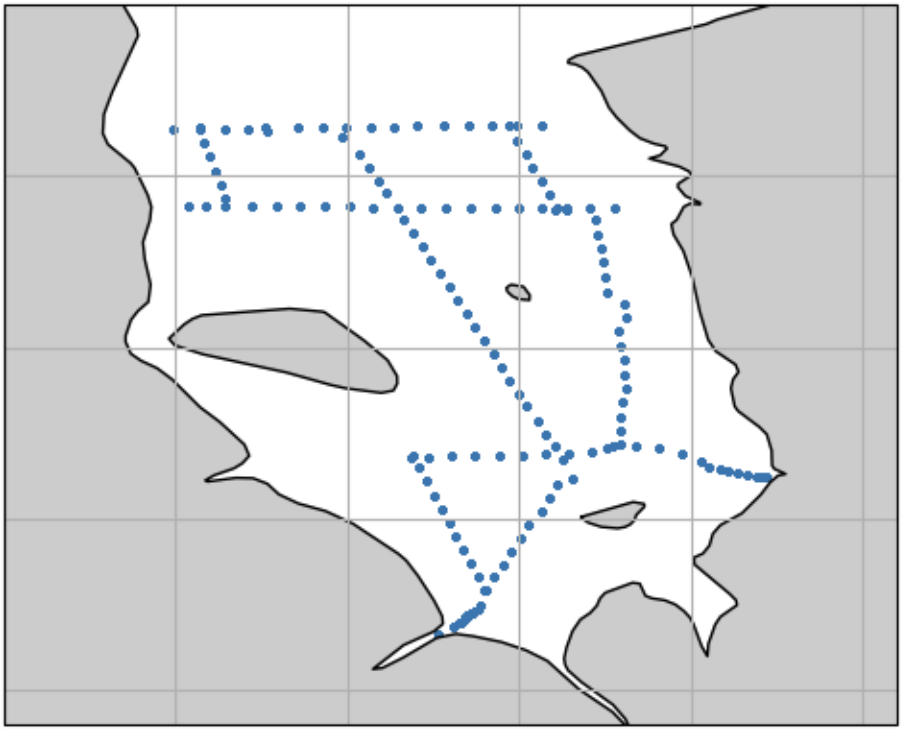

Figure 2.3: R/V William Kennedy observation locations for August 2021. Measurements were taken with a CTD instrument and over the course of 6 days from August 4 to August 9, 2023. Model points are taken from the nearest 5-day averages to encompass August 4 through 9. The 5-day averages thus chosen are model days August 3, 2021 and August 8, 2021, where the naming day is the middle day in the 5-day average.

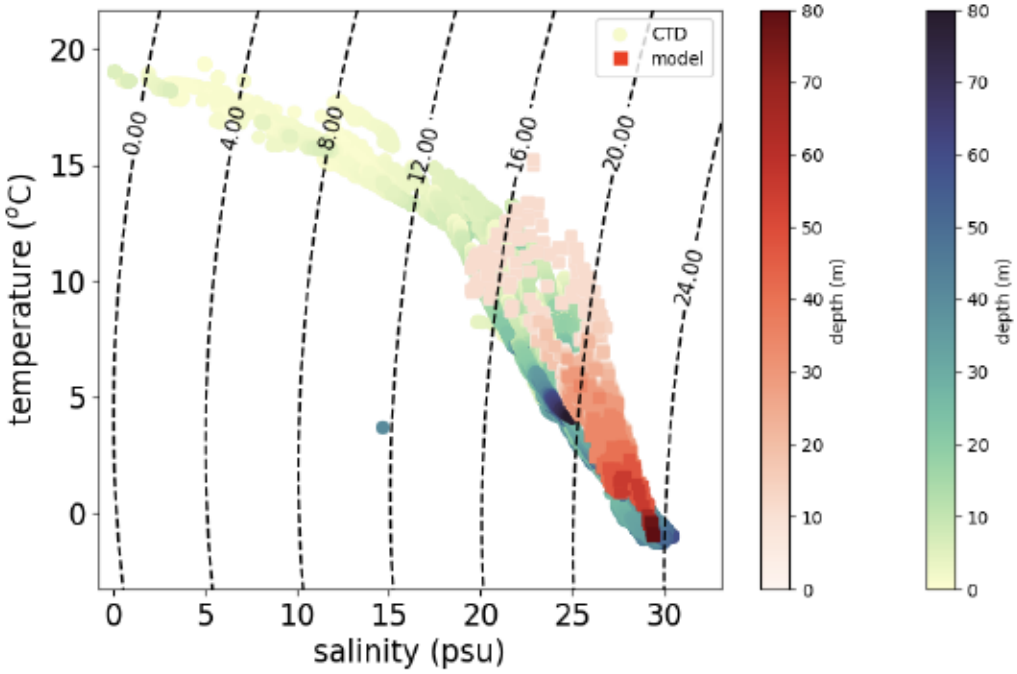

Figure 2.4: Temperature vs Salinity (TS) diagram for August 2021 CTD observations from the R/V William Kennedy. The isopycnals (lines of constant density in kg/m^3 are shown in dashed lines). The red shaded squares are the nearest model points to the observations, which are shown as blue-green circles. The shading for both model and observations gets darker with depth. An outlier point can be seen at T=5^{o}C and S=15 psu. This is likely an instrument error, but was chosen to be included in the plot.

Bibliography

[1] Nunavut Cambridge Bay. "Elder's Conference on Climate Change". In: (2001).

[2] ZA Kuzyk and LM Candlish. "From science to policy in the greater Hudson Bay marine region: An integrated regional impact study (IRIS) of climate change and modernization". In: *ArcticNet, Québec City* (2019), p. 424.

[3] Environment Canada and Climate Change. *Government of Canada*. Nov. 2017. URL: https://www.canada.ca/en/environment-climate-change/services/freshwater-quality-monitoring/hudson-bay-watershed.html.

[4] RG Ingram and S Prinsenberg. "Coastal oceanography of Hudson Bay and surrounding eastern Canadian Arctic waters". In: *The sea* 11.29 (1998), pp. 835–859.

[5] Simon J Prinsenberg. *Analytical study of the circulation of James Bay*. Fisheries and Environment Canada, 1978.

[6] Ran Tao and Paul G Myers. "Modelling the advection of pollutants in the Hudson Bay complex". In: *Journal of Marine Systems* 214 (2021), p. 103474.

[7] Miriam Anne McDonald, Lucassie Arragutainaq, and Zacharassie Novalinga. "Voices from the Bay: Traditional ecological knowledge of Inuit and Cree in the Hudson Bay bioregion". In: *(No Title)* (1997).

[8] Natasha A Ridenour et al. "Hudson Strait inflow: Structure and variability". In: *Journal of Geophysical Research: Oceans* 126.9 (2021), e2020JC017089.

[9] Igor A Shiklomanov and Alexander I Shiklomanov. "Climatic change and the dynamics of river runoff into the Arctic Ocean". In: *Water Resources* 30 (2003), pp. 593–601.

[10] Natasha A Ridenour et al. "Revisiting the circulation of Hudson Bay: Evidence for a seasonal pattern". In: *Geophysical Research Letters* 46.7 (2019), pp. 3891–3899.

[11] CD Smith et al. "CanCoast: A national-scale framework for characterizing Canada's marine coasts". In: *11th International Symposium for GIS and Computer Cartography for Coastal Zone Management*. 2013.

[12] A-M Hayden et al. "Multi-Century Impacts of Ice Sheet Retreat on Sea Level and Ocean Tides in Hudson Bay". In: *Journal of Geophysical Research: Oceans* 125.11 (2020), e2019JC015104.

[13] Peter S Galbraith and Pierre Larouche. "Reprint of "Sea-surface temperature in Hudson Bay and Hudson Strait in relation to air temperature and ice cover breakup, 1985–2009"". In: *Journal of Marine Systems* 88.3 (2011), pp. 463–475.

[14] Jennifer V Lukovich et al. "Simulated impacts of relative climate change and river discharge regulation on sea ice and oceanographic conditions in the Hudson Bay Complex". In: *Elem Sci Anth* 9.1 (2021), p. 00127.

[15] Roman V Bekryaev, Igor V Polyakov, and Vladimir A Alexeev. "Role of polar amplification in long-term surface air temperature variations and modern Arctic warming". In: *Journal of Climate* 23.14 (2010), pp. 3888–3906.

[16] Mika Rantanen et al. "The Arctic has warmed nearly four times faster than the globe since 1979". In: *Communications Earth & Environment* 3.1 (2022), p. 168.

[17] Walter N Meier and Julienne Stroeve. "An updated assessment of the changing Arctic sea ice cover". In: *Oceanography* 35.3/4 (2022), pp. 10–19.

[18] Benjamin Richaud et al. "Drivers of marine heatwaves in the Arctic Ocean". In: *Journal of Geophysical Research: Oceans* 129.2 (2024), e2023JC020324.

[19] Alistair J Hobday et al. "A hierarchical approach to defining marine heatwaves". In: *Progress in oceanography* 141 (2016), pp. 227–238.

[20] Eric CJ Oliver et al. "Marine heatwaves". In: *Annual review of marine science* 13 (2021), pp. 313–342.

[21] John R Moisan and Pearn P Niiler. "The seasonal heat budget of the North Pacific: Net heat flux and heat storage rates (1950–1990)". In: *Journal of Physical Oceanography* 28.3 (1998), pp. 401–421.

[22] Ce Bian et al. "Oceanic mesoscale eddies as crucial drivers of global marine heatwaves". In: *Nature communications* 14.1 (2023), p. 2970.

[23] Fernando P Lima and David S Wethey. "Three decades of high-resolution coastal sea surface temperatures reveal more than warming". In: *Nature communications* 3.1 (2012), p. 704.

[24] Eric CJ Oliver. "Mean warming not variability drives marine heatwave trends". In: *Climate Dynamics* 53.3 (2019), pp. 1653–1659.

[25] Gurvan Madec et al. "Ocean general circulation model reference manual". In: *Note du Pôle de modélisation* (1997).

[26] Martin Vancoppenolle et al. "The Louvain-la-Neuve sea ice model". In: *Notes du pole de modélisation, Institut Pierre-Simon Laplace (IPSL), Paris, France* 31 (2012).

[27] JL Bamber et al. "Land ice freshwater budget of the Arctic and North Atlantic Oceans: 1. Data, methods, and results". In: *Journal of Geophysical Research: Oceans* 123.3 (2018), pp. 1827–1837.

[28] Fedor Mesinger and Akio Arakawa. "Numerical methods used in atmospheric models". In: (1976).

[29] Andre J Robert. "The integration of a low order spectral form of the primitive meteorological equations". In: *Journal of the Meteorological Society of Japan. Ser. II* 44.5 (1966), pp. 237–245.

[30] Richard Asselin. "Frequency filter for time integrations". In: *Monthly Weather Review* 100.6 (1972), pp. 487–490.

[31] Gurvan Madec et al. "NEMO ocean engine". In: (2017).

[32] William George Large and Stephen G Yeager. *Diurnal to decadal global forcing for ocean and sea-ice models: The data sets and flux climatologies*. 2004.

[33] Thierry Fichefet and MA Morales Maqueda. "Sensitivity of a global sea ice model to the treatment of ice thermodynamics and dynamics". In: *Journal of Geophysical Research: Oceans* 102.C6 (1997), pp. 12609–12646.

[34] Ralph Timmermann et al. "On the representation of high latitude processes in the ORCA-LIM global coupled sea ice–ocean model". In: *Ocean Modelling* 8.1-2 (2005), pp. 175–201.

[35] Sylvain Bouillon et al. "An elastic–viscous–plastic sea ice model formulated on Arakawa B and C grids". In: *Ocean Modelling* 27.3-4 (2009), pp. 174–184.

[36] WD Hibler III. "A dynamic thermodynamic sea ice model". In: *Journal of physical oceanography* 9.4 (1979), pp. 815–846.

[37] Elizabeth C Hunke and John K Dukowicz. "The elastic–viscous–plastic sea ice dynamics model in general orthogonal curvilinear coordinates on a sphere—Incorporation of metric terms". In: *Monthly Weather Review* 130.7 (2002), pp. 1848–1865.

[38] Laura C Gillard. "Modelling the Interconnection of the Ocean and the Greenland Ice Sheet". In: (2021).

[39] *Mercator Ocean*. `https://www.mercator-ocean.eu/en/ocean-science/glorys/`. Accessed: 2024-06-10.

[40] Michael Steele, Rebecca Morley, and Wendy Ermold. "PHC: A global ocean hydrography with a high-quality Arctic Ocean". In: *Journal of Climate* 14.9 (2001), pp. 2079–2087.

[41] Seiji Yukimoto et al. "A new global climate model of the Meteorological Research Institute: MRI-CGCM3—Model description and basic performance—". In: *Journal of the Meteorological Society of Japan. Ser. II* 90.0 (2012), pp. 23–64.

[42] A Dai. *Dai and Trenberth Global River Flow and Continental Discharge Dataset [Dataset].* Accessed: 2024-06-10. 2017. DOI: https://doi.org/10.5065/D6V69H1T.

[43] TA Stadnyk et al. *Hydrological modeling of freshwater discharge into Hudson Bay using HYPE. Elem. Sci. Anthr. 8.* 2020.

[44] Christiaan T van Dalum et al. "First results of the polar regional climate model RACMO2. 4". In: *EGUsphere* 2024 (2024), pp. 1–36.

[45] Gregory C Smith et al. "A new atmospheric dataset for forcing ice–ocean models: Evaluation of reforecasts using the Canadian global deterministic prediction system". In: *Quarterly Journal of the Royal Meteorological Society* 140.680 (2014), pp. 881–894.

[46] Tahya WeissGibbons et al. "Increased runoff from Siberian rivers leads to Arctic wide freshening". preprint available at https://essopenarchive.org/users/659901/articles/663686-increased-runoff-from-siberian-rivers-leads-to-arctic-wide-freshening.

[47] *Advanced Microwave Scanning Radiometer 2 (AMSR2).* https://www.earthdata.nasa.gov/learn/find-data/near-real-time/amsr2. Accessed: 2024-07-08.

[48] *Southern Hudson Bay - James Bay CTD Data 2021.* https://canwin-datahub.ad.umanitoba.ca/data/dataset/hudson-bay-james-bay-ctd-2021. Accessed: 2024-07-08.

[49] *Kiel Climate Model System.* https://www.geomar.de/kcms. Accessed: 2024-07-12.

[50] *WMO guidelines on the calculation of climate normals.* Doc. WMO-No. 1203, WMO, Geneva. 2017.

[51] Alistair J Hobday et al. "Categorizing and naming marine heatwaves". In: *Oceanography* 31.2 (2018), pp. 162–173.

[52] *NCEP/DOE Reanalysis II.* ttps://psl.noaa.gov/data/gridded/data.ncep.reanalysis2.tml. Accessed: 2024-06-42.

[53] Daqing Yang et al. "Heat flux, water temperature and discharge from 15 northern Canadian rivers draining to Arctic Ocean and Hudson Bay". In: *Global and Planetary Change* 204 (2021), p. 103577.

Chapter 3

Results

Reports of extreme climatic events in Hudson Bay and James Bay have been ongoing since the 1990s [2]. Those reports include decline in eelgrass meadows, warmer and shorter winters, and erratic weather and sea ice patterns. Among these extreme and erratic events are Marine Heatwaves (MHWs). It is still an open question if MHWs play a role in the initiation or duration of these other climatic changes, like decline in eel grass meadows or unusual sea ice patterns. This chapter will focus on exploring the dynamics of MHWs in southern Hudson Bay and James Bay (SHBJB) using numerical ocean models. Each experiment listed in table 3.1 is analysed with a MHW lens. EPM151 is analysed as the baseline for the two sensitivity experiments— EPM111 and ETW161— which will determine the role of atmospheric forcing and river runoff temperature. To parse of the mechanisms of MHW in SHBJB, each term in equation 3.1 is calculated with the model output to look at the processes that may play a role in the warming associated with a marine heat wave. The analysis starts with calculating the horizontal advection of the model output in section 3.3.2, then in section 3.3.3, the air-sea heat fluxes are investigated further.

In equation 3.1, T is the temperature of the mixed layer, $\mathbf{u}$ is the two-dimensional horizontal ocean velocity, w is the vertical velocity, h is the depth of the mixed layer, κ_h and κ_z are

Experiment	Integration	IC	BC	Atmospheric Forcing	Runoff
EPM151	2002-2022	GLORYS2v3	GLORYS2v3	CGRF	A-HYPE/B18
EPM111	1958-2022	PHC3.0	Kiel_K3415	CORE-IA	DT/B18
ETW161	2002-2018	GLORYS2v4	GLORYS2v4	CGRF	A-HYPE/B18

Table 3.1: Model runs used in this thesis and their setup. Column 3 lists the configuration initial conditions, where GLOYS2v3 come from the Mercator Ocean Team [39] and PHC comes from the Polar Science Center [40]. Column 4 lists the boundary conditions, where Kiel comes from Geomar climate model [49]. For runoff DT is the Dai and Trenberth [42], B18 is Bamber [27] Greenland runoff., and A-HYPE is the Arctic implementation of the HYdrological Predictions for the Environment (HYPE) hydrological model [43]

.

the horizontal and vertical diffusivity coefficients, ρ and c_p are the density and specific heat capacity of seawater, respectively, and Q encompasses each different term for the air-sea heat flux— the shortwave (Q_{SW}) and longwave (Q_{LW}) radiation as well as the turbulent latent (Q_{lat}) and sensible (Q_{sens})heat fluxes. This equation simplifies equation 1.1 and describes how different physical processes, such as horizontal advection, air-sea heat flux, and vertical mixing, affect the rate of change of temperature in the mixed layer via the transfer of heat [20].

$$\frac{\partial \overline{T}}{\partial t} = -\overline{\mathbf{u}} \cdot \nabla \overline{T} \; + \; \frac{Q_{SW} \; + \; Q_{SW\,(-h)} \; + \; Q_{LW} \; + \; Q_{sens} \; + \; Q_{lat}}{\rho c_p h} \; + \; residual \tag{3.1}$$

3.1 Methods

The net air-sea heat flux (Q_{net})is given by the following equation:

$$Q_{net} = Q_{SW} + Q_{LW} + Q_{sens} + Q_{lat} \tag{3.2}$$

where Q_{sw} is the heat flux from incoming shortwave radiation, Q_{lw} is from the longwave radiation, Q_{sens} is the sensible heat flux, and Q_{lat} is the latent heat flux. The shortwave radiative flux leaving the bottom of the mixed layer is neglected due to the shallow depths of

the study region. The shortwave radiation flux is provided solely by the atmospheric forcing product (table 3.1). The NEMO model has different turbulent heat flux formulations built in. In this thesis, all model experiments use the COREBULK formula [32] to calculate turbulent fluxes. This formula describes the exchange of heat between atmosphere and ocean depending on their temperatures, humidity, velocities, and drag coefficients. Below is the COREBULK formulation, with ice concentration taken out of account.

$$Evap = \rho_a C_E \left(q(z_q) - q_{sat}(SST)\right) |\Delta \mathbf{U}| \tag{3.3}$$

$$Q_{lat} = L_v \times Evap \tag{3.4}$$

$$Q_{sens} = \rho_a c_p C_H \left(\theta(z_\theta) - SST\right) |\Delta \mathbf{U}| \tag{3.5}$$

where ρ_a is the density of air near the surface ($\rho_a = 1.22 kg/m^3$), C_E is the transfer coefficient for evaporation, C_H is the sensible heat, $q(z_q)$ is the specific humidity at height equal to z, $|\Delta \mathbf{U}|$ is the wind modulus, L_v is the latent heat of vaporization, $\theta(z_\theta)$ is the potential air temperature, c_p is the specific heat capacity, q_{sat} is the specific humidity of saturated air given by the following formula:

$$q_{sat}(q_1, q_2, SST) = \rho_a^{-1} \left(0.98 \times 640380 \frac{kg}{m^3}\right) e^{\frac{-5107.4K}{SST}} \tag{3.6}$$

where the coefficients $q_1 = 0.98 \times 640380 kg/m^3$ and $q_2 = -5107K$, and the factor 0.98 is only applied over sea water [32]. The long wave radiation (shown below) is given by the non-solar heat flux, i.e., the long wave radiation coming from the atmosphere, clouds, etc., minus the blackbody radiation emitted by the ocean, given by the Stefan-Boltzmann law.

$$Q_{lw} = Q_{lw}^{atmos} - \sigma T^4 \tag{3.7}$$

3.2 Data

Atmospheric forcing data is provided by the Canadian Meteorological Centre Global Deterministic Prediction System ReForecasts (CGRF), derived from the global deterministic prediction system (GDPS). This is reforecast data, as opposed to reanalysis, meaning that it is simply operational forecasts from the GDPS model [45], but is produced in a consistent manner. Other atmospheric forcing datasets for hindcasts include reanalysis data from the coordinated ocean-ice reference experiments version 2 (CORE-IA). For initial conditions and boundary conditions in EPM151— as well as for ETW161— GLORYS $\frac{1}{4}^o$ reanalysis from Mercator Ocean is used. Here, ocean model output is combined with existing observations to synthesize an estimate of the state of the ocean. For EPM111, boundary conditions are derived from Geomar's Kiel eOCRA025 ocean model [49], based on NEMO. Initial conditions for EPM111 uses Polar Science Center Hydrographic Climatology (PHC), which merges the World Ocean Atlas observational data with data from the Arctic Ocean Atlas, thus creating a more comprehensive global climatology with better representation of the Arctic Ocean [40].

For EPM151 runoff is provided by A-HYPE and for EPM111, runoff is provided by Dai and Trenberth [42] which has monthly river runoff data from 925 of the worlds largest rivers as well as continental discharge rates, but fails to include any interannual variability after 2007. For all experiments, Greenland runoff is provided separately by Bamber 2018 [27] which is derived from a combination of climate model, satellite, and terrestrial data. For ETW161, river runoff is provided by the A-HYPE hydrological model [43], developed specifically for the Arctic and Hudson Bay drainage system. River heat is included with the discharge in

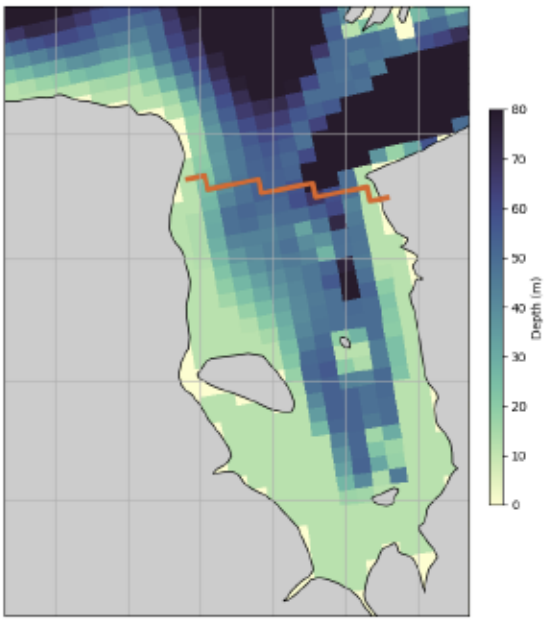

Figure 3.1: Southern Hudson Bay and James Bay analysis region with depth contoured on top. The orange line indicates the transect at the "mouth" of James Bay in which all transports are calculated across.

ETW-161, providing a more realistic model representation than previous experiments, which input river discharge at the same temperature as the ocean near the river mouth [46] [in review].

3.3 Marine Heatwaves in James Bay, Canada

In this section, we will discuss the Marine Heatwave (MHW) analysis performed for Southern Hudson Bay and James Bay (SHBJB), Canada. Analysis performed on model run EPM151 is presented first and represents a "baseline" to compare all other model run analysis. All analysis is performed on the region similar to that shown in figure 3.1.

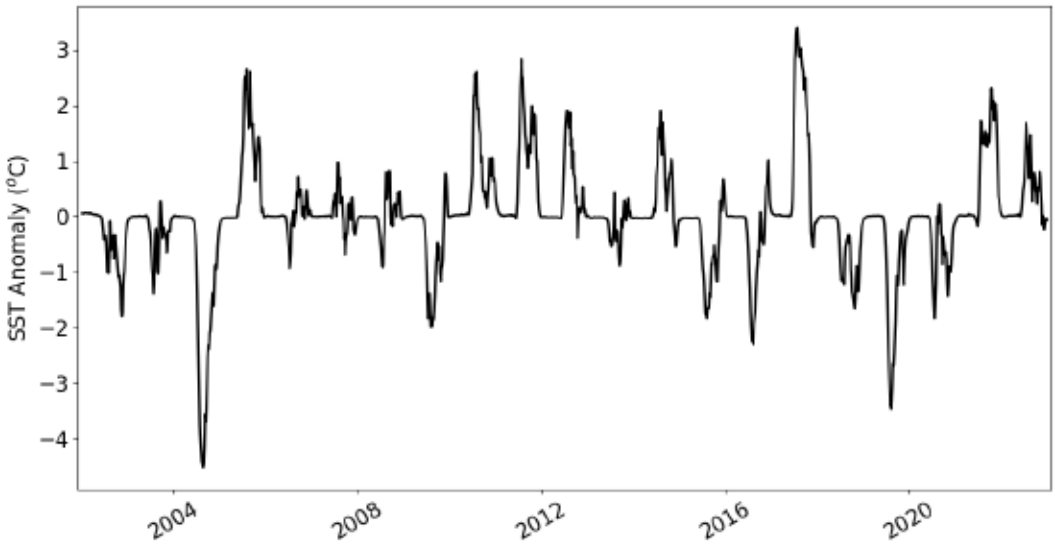

Figure 3.2: SST anomaly in degrees Celsius in SHBJB for model run EPM151 for year 2002 to the end of 2022. MHW signatures can be seen in 2005, 2011, 2017, for example, with anomaly values of approximately 2.7, 3, and 3.3 degrees Celsius, respectively. Also shown in the plot are Marine Cold Spells (MCS), most noticeably in 2004 and 2019, with values of -4.6 and -3.5 degrees Celsius, respectively.

3.3.1 SST Analysis

In this MHW analysis, the "climate signal" is be subtracted from the Sea Surface Temperature (SST) to get a time series of the SST anomaly. Normally in climate studies, climatological timescales are taken to be 30 year averages, as commonly seen by NASA and the International Panel on Climate Change (IPCC) [50]. However, this model experiment only has a 20 year time integration. Thus, 2002-2022 is taken to be the climatological period. Shown in Figure 3.2 is the SST anomaly for EPM151. These anomalies are defined relative to the regional average SST of the whole time series. The region is southern Hudson Bay and James Bay and it is defined by a mask region that encompasses an area similar to that shown in Figure 3.1. From this figure, certain years already stand out as possible MHW events— notably, 2005 and 2017, with summertime anomalies of 2.5 ^{o}C and 3.4 ^{o}C, respectively.

Another phenomenon shows up when analyzing SST data— Marine Cold Spells (MCS). MCS

have an analogous definition to MHWs, but occur when there is prolonged ocean temperature distribution below a low percentile threshold [20]. This phenomenon is also significant in terms of it's negative affects on the health of the ecosystem, however, MCS are beyond the scope of this thesis and will not be discussed further.

3.3.2 Horizontal Advection

The subsequent sections look closer into the processes associated with MHWs. First, horizontal advection, given by $-\overline{\mathbf{u}} \cdot \nabla \overline{T}$ in equation 3.1, is calculated using model output. Figure 3.3 shows the horizontal advection for model run EPM151 for the whole time series. Note the directionality: positive denotes advection out of the region and negative denotes advection into the region (SHBJB, refer to fig. 3.1). A similar directionality applies to figure 3.4. This is the heat transport across the mouth of James Bay. From these plots, certain years show seemingly significant heat transport and advection into James Bay— given that the directionality is the same for both the same, if there is high transport into the bay, there will also be high heat advected into the region. Figure 3.2 shows that the year 2017 stands out as a year with high amounts of heat coming into the bay, which will be discussed further in section 3.4.2.

In 2017, there is a large influx of heat into the bay, which is also a year with some of the lowest sea ice concentrations in EPM151, as shown in Figure 3.5, with a winter (JFMA) average ice concentration of 0.92 over SHBJB. Here, the ice concentration is taken to be the fraction or percentage of a grid cell covered by sea ice.

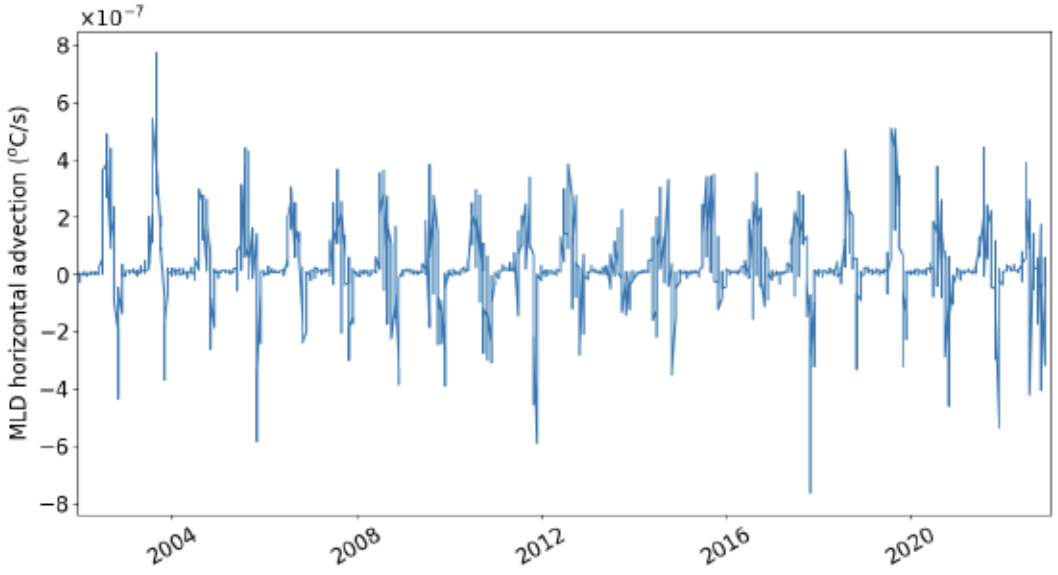

Figure 3.3: EPM151 monthly regional (SHBJB) averages of horizontal advection in degrees Celsius per second in the mixed layer depth (MLD) from 2002-2022. Negative indicated advection into the region (James Bay), whereas positive indicates advection out of the region.

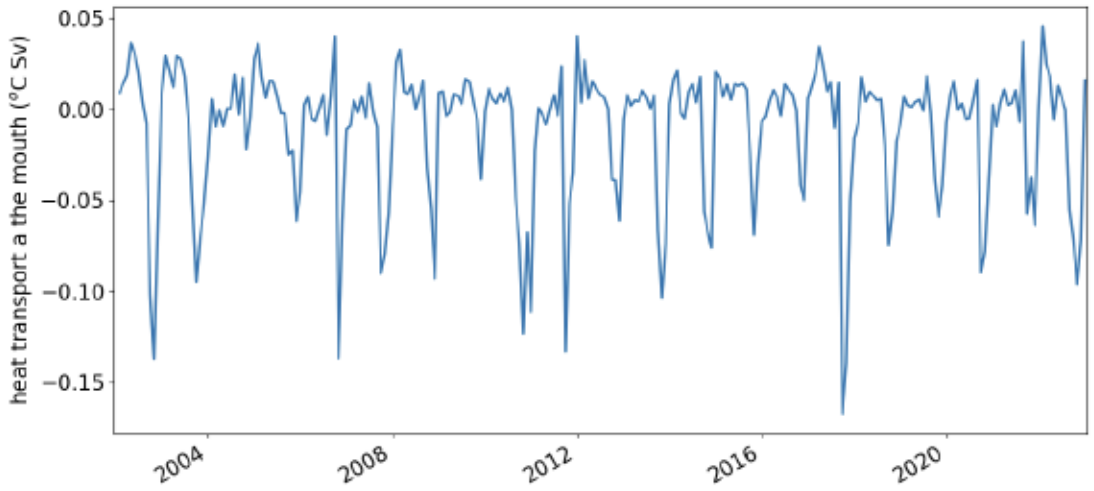

Figure 3.4: Heat transport (degrees Celsius times Sverdrup) at the mouth of James Bay for EPM151. Negative sign indicates (southward) transport into the bay, whereas positive indicates (northward) transport out of the bay.

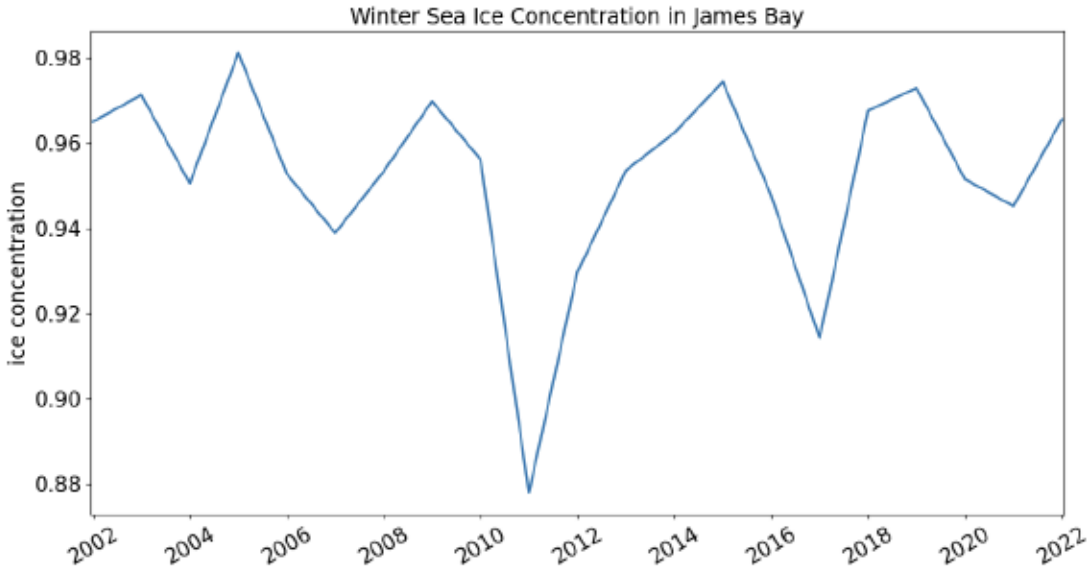

Figure 3.5: EPM151 sea ice concentration— as a fraction of a grid cell— regionally averaged for SHBJB in full ice cover months (January, February, March and April), spanning 2002 to the end of 2022.

3.3.3 Air-Sea Heat Fluxes

Air-sea heat flux, given by $\frac{Q_{net}}{\rho c_p h}$ in equation 3.1, can be calculated using model output using equation 3.1. Shown in Figure 3.6 and 3.7 is the calculated monthly averages of turbulent sensible and latent heat fluxes, respectively, for EPM151. Negative signs indicate heat flux from the atmosphere to the ocean, whereas positive signs indicate heat flux from ocean to atmosphere. Again, like with horizontal advection, some years stand out with particularly large heat fluxes into the ocean, such as large latent heat flux in 2017 and large sensible heat flux in 2012 or 2021.

The other terms that contribute to the air-sea heat flux are the radiative fluxes from the atmosphere. These include the incoming shortwave radiation and the longwave radiation. Shortwave radiation in the model penetrates into the ocean and decays with depth. The longwave radiation term must be calculated by subtracting the radiation that is emitted from the ocean into the atmosphere, as stated by the Stefan-Boltzman law, mentioned in

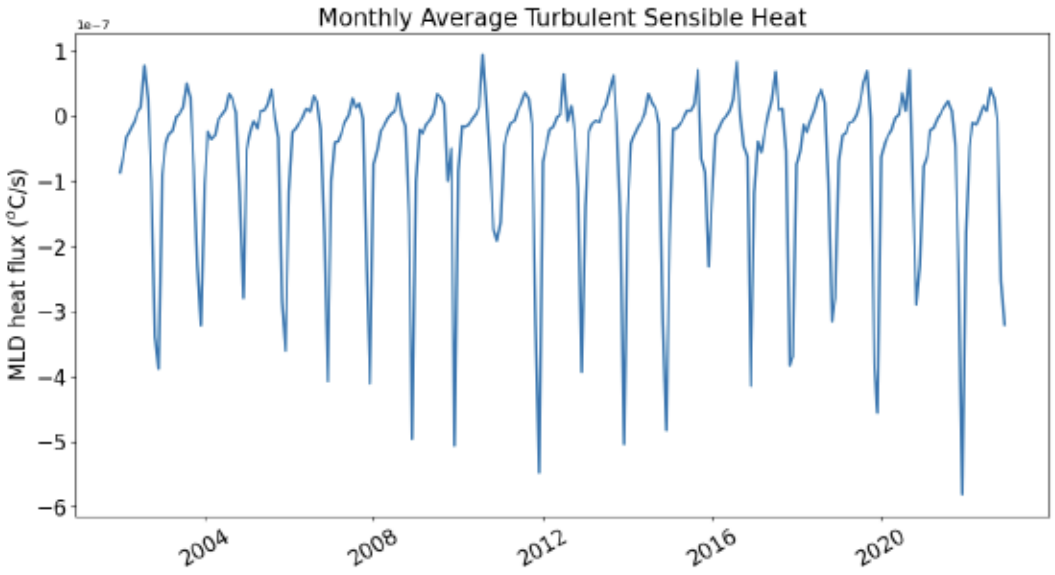

Figure 3.6: EPM151 turbulent sensible heat flux monthly regional averages calculated using the COREBULK formula (as discussed in the methods section) for years 2002 to the end of 2022. Units are Watts per meter squared. Negative signs indicate heat going from atmosphere to ocean, whereas positive signs indicate heat going from ocean to atmosphere.

chapter 2 of this thesis. All together, the radiative fluxes are shown in Figure 3.8. The directionality for radiative flux plots differ from previous plots. Here, positive indicates heat fluxes into the ocean— heating the ocean— and negative is heat fluxes to the atmosphere— cooling the ocean.

Notice the magnitude differences between radiative and turbulent heat fluxes. Based on this, any air-sea heat flux contributions to marine heatwaves likely will come mainly from the radiation terms, while the turbulent terms may act to either intensify or prolong events.

3.4 Case Studies

Looking at Figure 3.2, certain years stand out as particularly high SST anomalies and potential MHW events. Notably, the two highest anomaly years are 2005 and 2017 and have maximum anomaly values of 2.6^{o}C and 3.4^{o}C, respectively. This section will focus on these

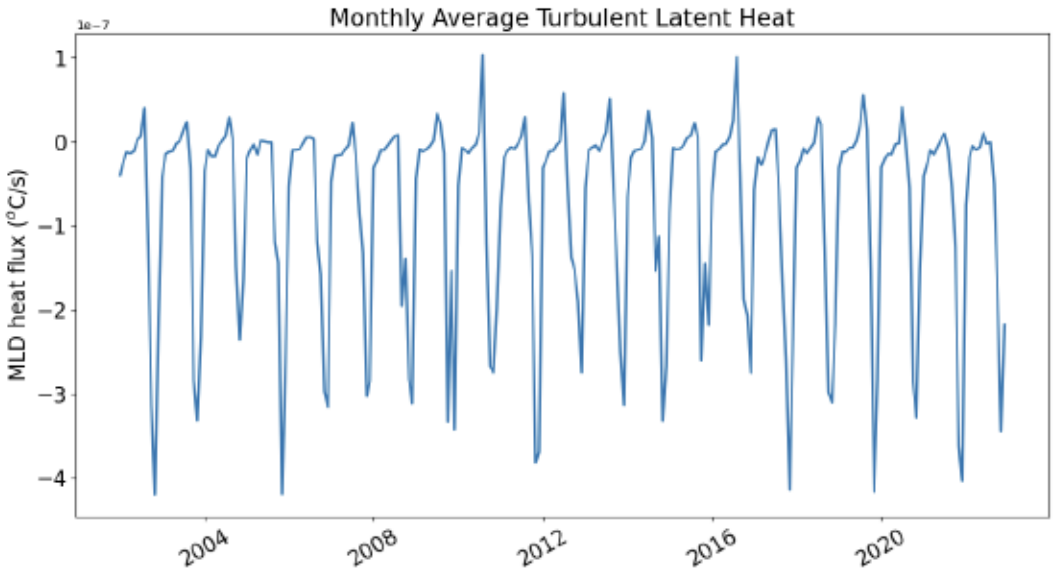

Figure 3.7: EPM151 turbulent latent heat flux (W/m^2) monthly regional averages calculated using the COREBULK formula— as mentioned in the methods— for 2002 to 2022. Directionality is similar to turbulent sensible heat flux.

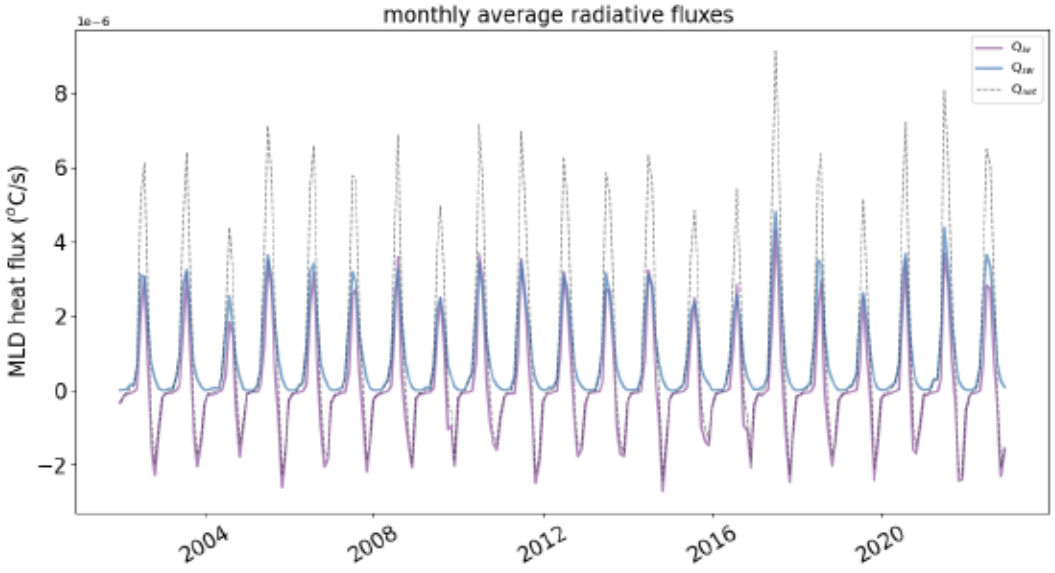

Figure 3.8: The monthly averages of shortwave, longwave, and total radiative heat fluxes (W/m^2) for EPM151 years 2002-2022. The purple solid line is the longwave radiation, the blue solid line is the shortwave radiation, and the dashed black line is the net radiation.

two years as case studies and look closer at the dynamics influencing these MHW events.

3.4.1 2005 MHW

In Figure 3.2, 2005 is the first year that stands out as a potential MHW event. Figure 3.9 shows the SST anomaly for 2005 as well as the first category MHW range, as defined by a local "5-day" upper-percentile climatology, similar to that described by Hobday [19][51] and Oliver [20]. With this definition of MHW events, the categories describe the intensity of the MHW event, with each category magnitude defined by the difference between the 90th percentile climatology and the baseline climatology, i.e., each category is a multiple of the 90th percentile difference. This is illustrated by the following equation:

$$\Delta T = T_{90} - T_c \tag{3.8}$$

Figure 3.9 shows the start of the MHW event early in the year when the ice cover melts with temperatures in and above the second category, 2ΔT. The rest of the year, temperatures swing in and out of the first MHW category, with anomalies peaks of around 3^oC occurring in August and September. Another peak as a category 1 MHW occurs in November, with temperature anomalies around 1.5^oC.

To further investigate the 2005 MHW, the dynamics can be parsed out and looked at closer. Figure 3.10 shows the calculated horizontal advection for 2005. Again, the directionality is such that negative indicates heat being advected into SHBJB region and positive is heat being advected outwards. This figure shows that almost no heat is being advected during the ice cover months, but as the ice melts, heat is advected outwards. However, during November, the direction switches and heat is then advected into the region. This shows that while horizontal advection may not be the initial driver of the MHW event early on in the

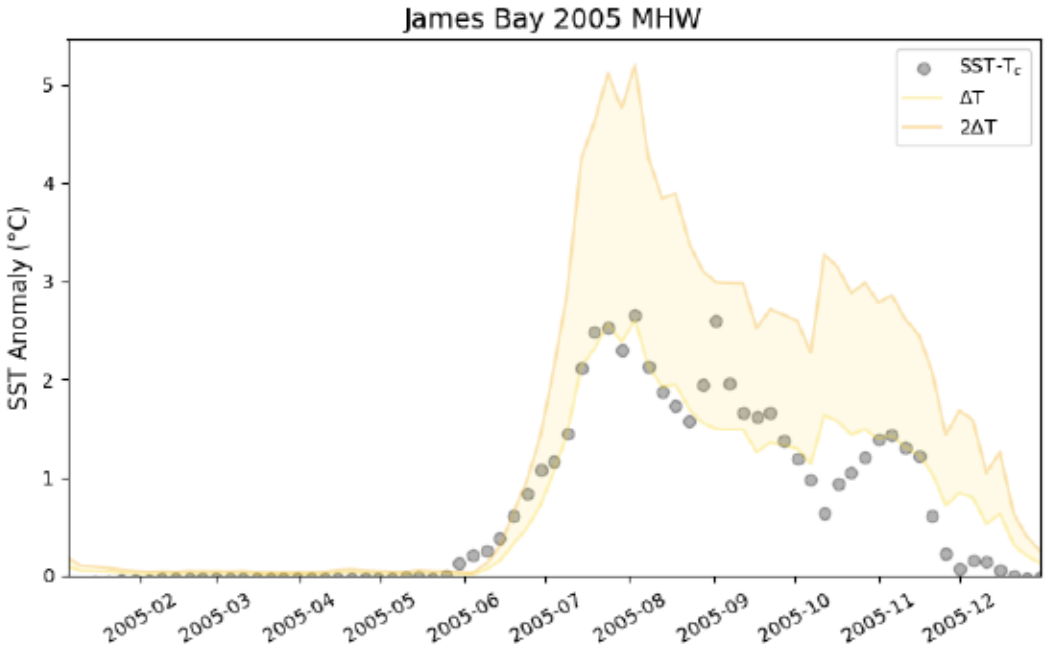

Figure 3.9: EPM151 2005 SST anomaly with units of degrees Celsius. The lower yellow solid line indicates the 90th percentile quantile difference— defined by equation 3.8— while the solid orange line on top indicates the second quantile. The shaded yellow region is the first category of MHW, with temperatures between the first and second MHW categories, $2\Delta T$-ΔT.

year, it is likely a driver of the final MHW event occurring later in the year. Figure 3.11 corroborates this explanation, as there is an uptick in heat being transported into the bay during the month of November.

Looking at the air-sea heat fluxes, Figures 3.13, 3.12, and 3.14 show the sensible, latent, and radiative heat fluxes, respectively. For sensible and latent fluxes, negative signs indicate heat flux from the atmosphere to the ocean, whereas positive signs indicate heat flux from ocean to atmosphere. Again, the sensible and latent heat fluxes are negligible up until the month of November, where heat flux is going into the ocean. This likely contributes to the MHW during that month. However, for the radiative fluxes, the directionality is opposite to that of latent and sensible. Figure 3.14 shows that the combination of both the long wave and short wave radiation, which onsets in May and peaks in July, is positive into the ocean, thus likely contributing the onset of the MHW during this year. It is also likely that the onset relates

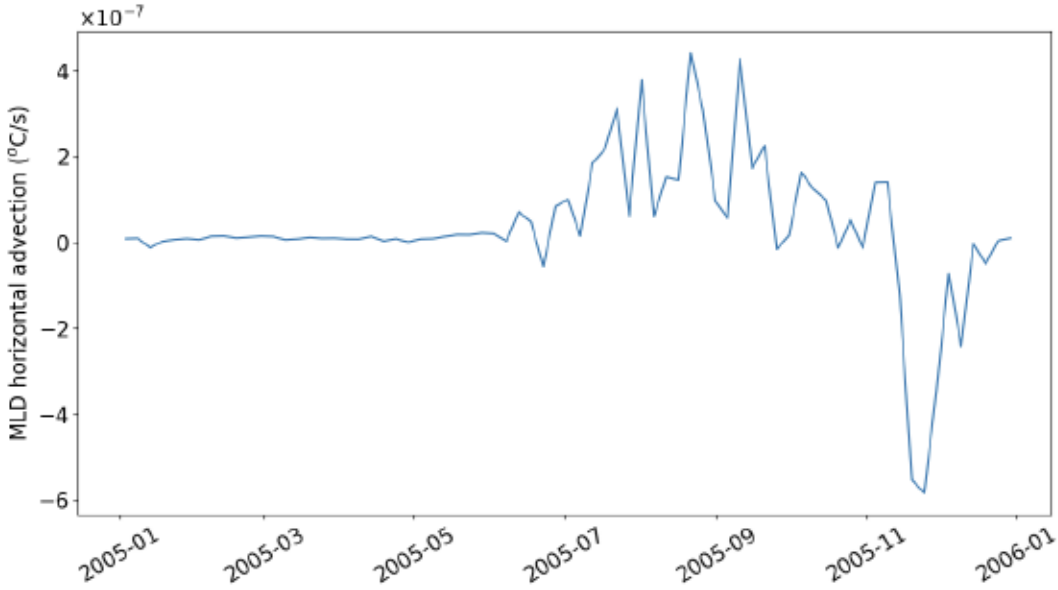

Figure 3.10: EPM151 horizontal advection (degrees Celsius per second) for 2005. Negative indicated advection into the region (James Bay), whereas positive indicates advection out of the region

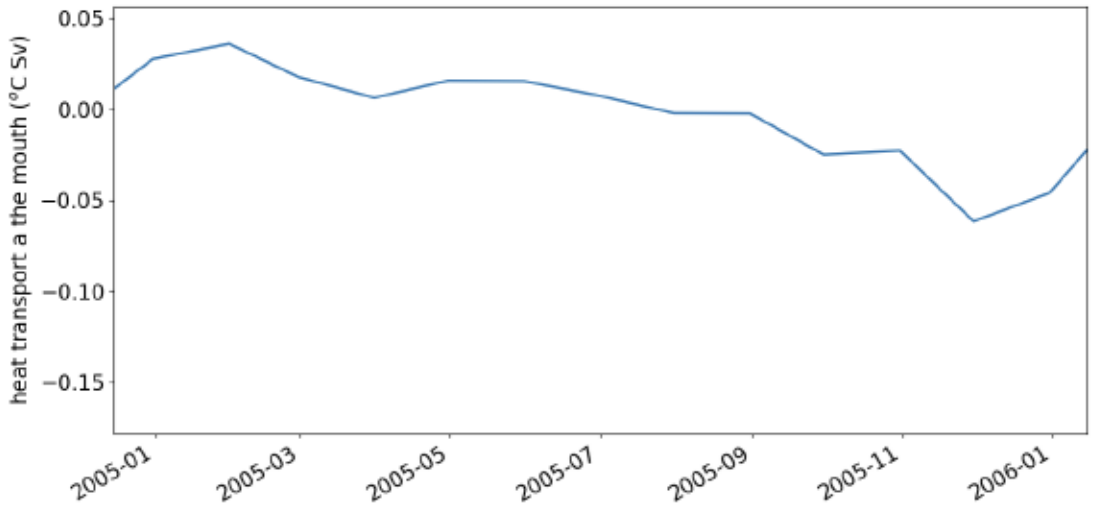

Figure 3.11: EPM151 heat transport at the mouth of James Bay, with units of °C Sv. Negative indicated advection into the bay, whereas positive indicates advection out of the region.

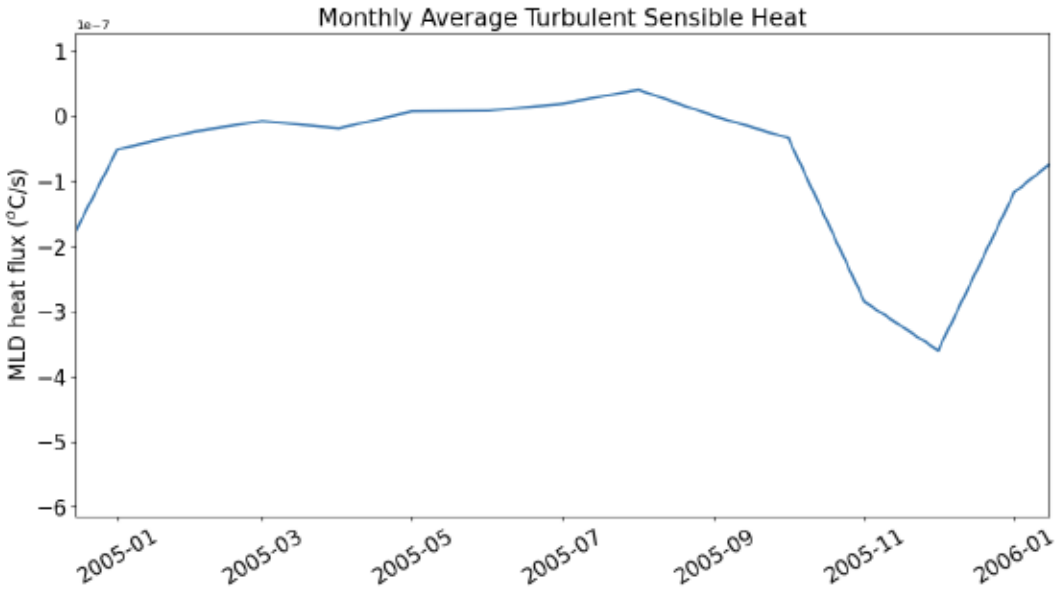

Figure 3.12: EPM151 turbulent sensible heat flux with units of W/m^2 for 2005. Negative signs indicate heat flux from the atmosphere to the ocean, whereas positive signs indicate heat flux from ocean to atmosphere.

to the ice breakup, which allows for more radiative heat flux to reach the ocean.

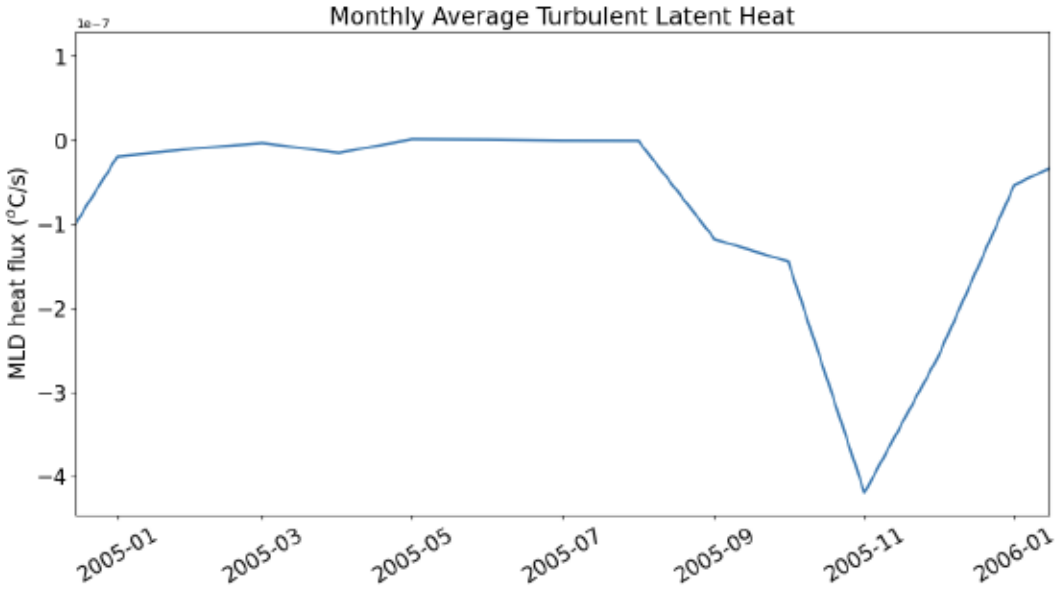

Figure 3.13: EPM151 turbulent latent heat flux with units of W/m^2 for 2005. The directionality is similar to that of previous figures.

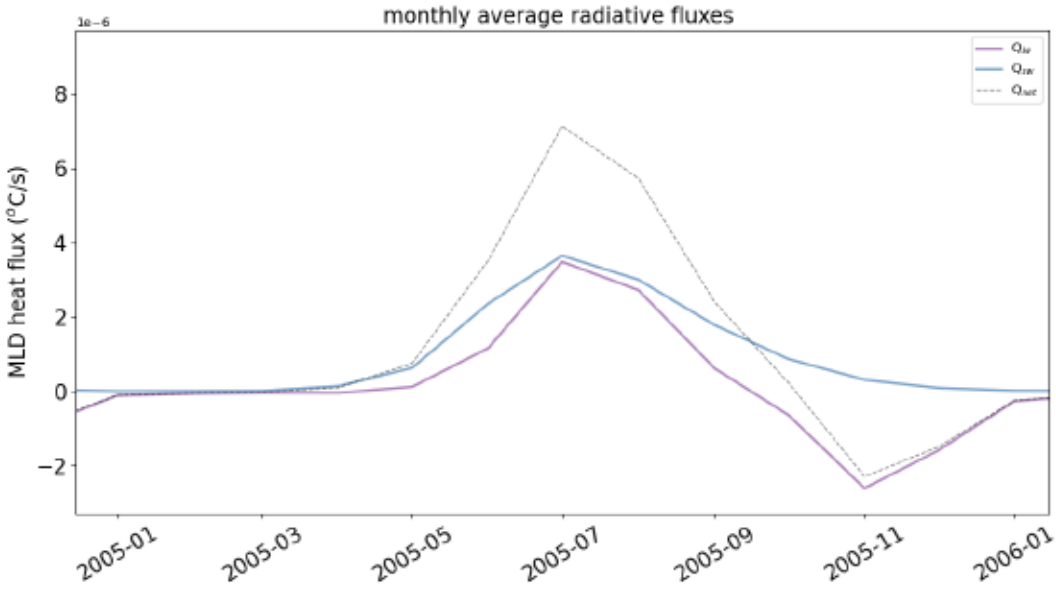

Figure 3.14: EPM151 2005 radiative fluxes with units in W/m^2. The purple solid line is the longwave radiation, the blue solid line is the shortwave radiation, and the dashed black line is the net radiation. The directionality for radiative flux plots differ than previous plots. Here, positive indicates heat fluxes into the ocean— heating the ocean— and negative is heat fluxes to the atmosphere— cooling the ocean.

3.4.2 2017 MHW

The second MHW case study focuses on the year 2017, which Figure 3.2 shows to have a peak over 3.54 °C. Taking a closer look at this year, Figure 3.15 shows the SST anomalies for 2017. Again, the categories are defined by equation 3.8 such that the yellow line is the first 90th percentile difference and the orange line is the second multiple of this difference.

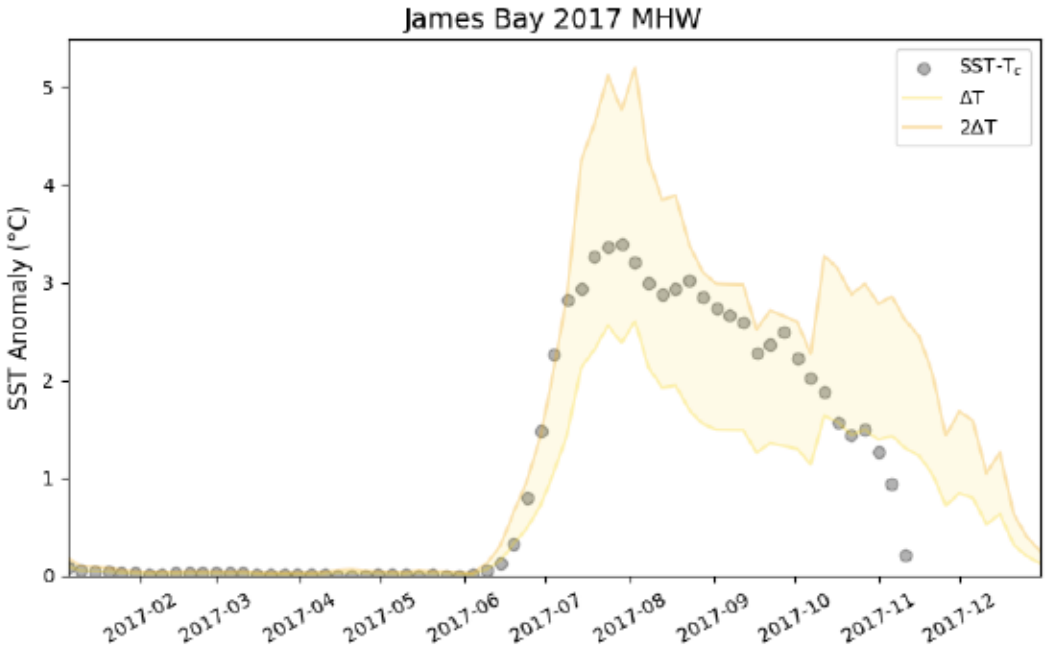

Figure 3.15: EPM151 2017 SST anomaly with units of degrees Celsius. The lower yellow solid line indicates the first percentile quantile, while the solid orange line on top indicates the second quantile. The shaded yellow region is the first category of MHW, with temperatures between the first and second quantile.

The MHW starts soon after the ice cover opens up in June and rises into a strong category 1 event. This event doesn't seem to let up and lasts most of the year before tapering out in November. Looking at Figure 3.16, a similar trend to 2005 is seen, where a large advection of heat into the bay occurs in October to November. Similarly, with latent heat, the largest influx of heat into the ocean occurs in November. This indicates that while horizontal advection and perhaps latent heat do not play a significant role in the onset of the 2017 MHW, they likely contribute to the prolonging of this event throughout the year and into

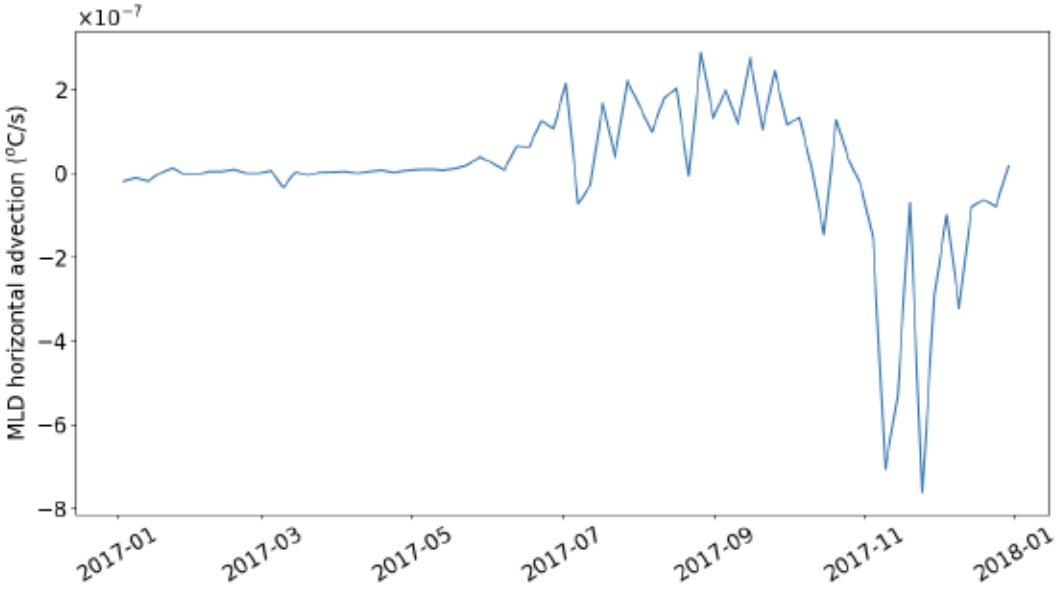

Figure 3.16: Horizontal advection for 2017

the winter.

That leaves the final piece of the puzzle: where does this 2017 MHW come from? Looking at Figure 3.18, it shows a strong influx of heat, both long wave and short wave, into the ocean starting in May and tapering off into the fall. Therefore, radiative fluxes are likely the driver of the 2017 MHW. Note the directionality difference shows that the radiative fluxes don't contribute to the prolonging of the MHW into the winter, rather it opposes the other drivers and helps diminish it.

3.5 Overview

The analysis of model run EPM151 has shown SST anomalies— comparing to a 20-year model climatology— in which certain years stand out as possible MHW events. The analysis also included calculating the different driver terms in equation 3.1, starting with the horizontal advection, then looking at how the atmospheric forcing influences the ocean heat by way of

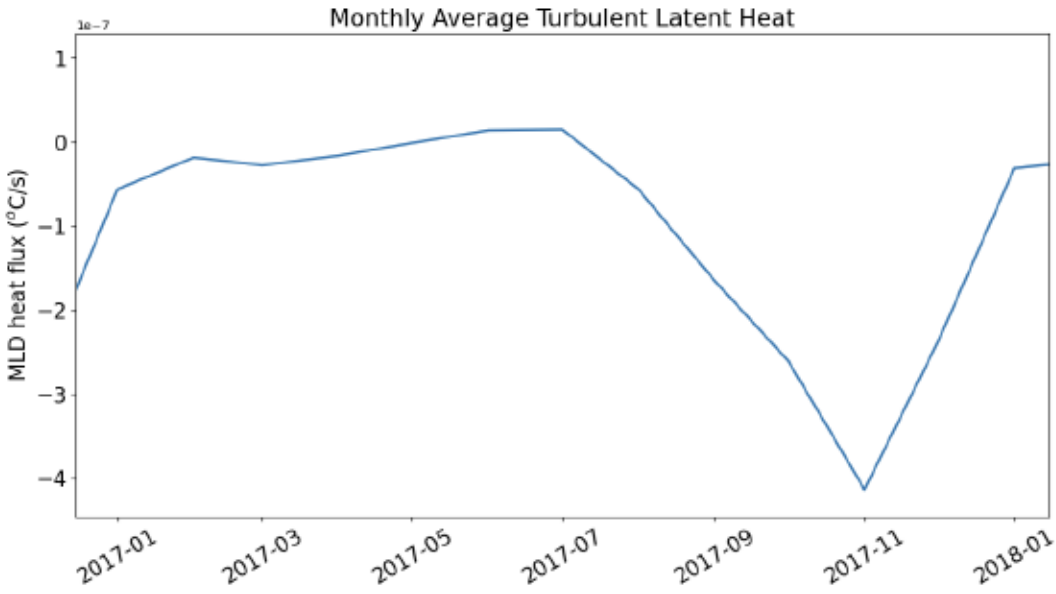

Figure 3.17: EPM151 turbulent latent heat flux with units of W/m^2 for 2017.

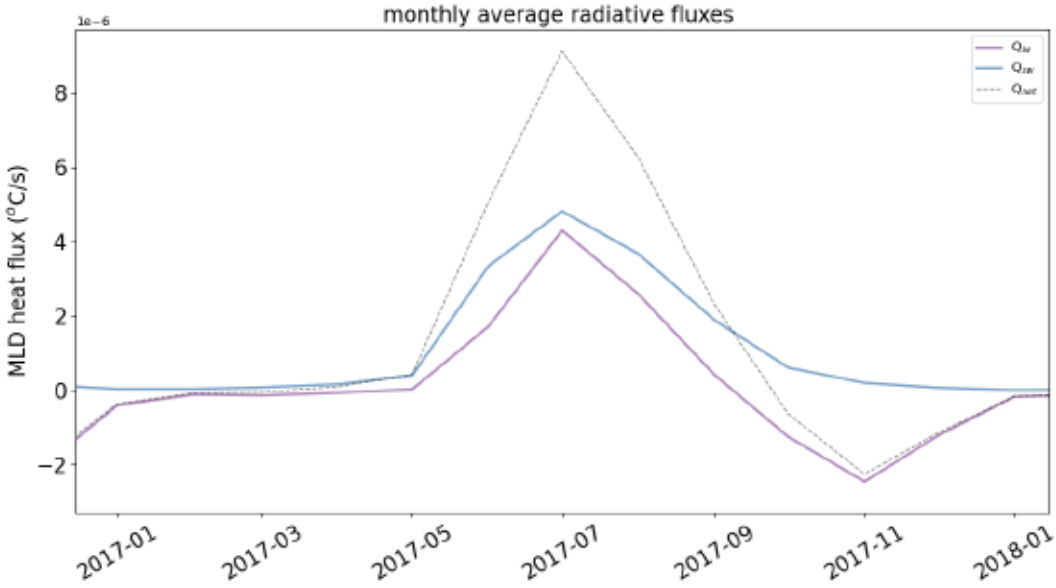

Figure 3.18: EPM151 2017 radiative fluxes with units in Watts per meter squared. The purple solid line is the long wave radiation, the blue solid line is the shortwave radiation, and the dashed black line is the net radiation.

air-sea fluxes. Lastly, two case study years were picked out from Figure 3.2, picking the years with the highest anomalies— 2005 and 2017— with maximum values of 2.6 ^{o}C and 3.4^{o}C, respectively.

The year 2005 shows that horizontal advection, as well as turbulent latent and sensible heat fluxes may have acted to drive the MHW event occurring in November. However, both the long wave and shortwave radiative fluxes onset in May and peak in July, showing that this is likely the initial driver of the MHW that starts early in the spring and continues into the summer.

In 2017, a MHW starts soon after the ice cover melts in the bay and continues as a category 1 MHW far into the year until decaying in November. Again, the horizontal advection and turbulent heat fluxes are small until the late fall, which likely then act to prolong this MHW event until the winter. It is again the radiative fluxes that are the initial driver that onset the MHW event soon after the ice cover melts.

3.6 Sensitivity Experiments

To expand on this MHW analysis, sensitivity experiments can be done to identify the influence of changing the atmospheric forcing, as well as adding river heat to the ocean. The first sensitivity study done is to change the atmospheric forcing dataset, choosing to use a combination of CORE2-IA and NCEP-R2 reanalysis data instead of the CGRF reforecast. The second sensitivity study involves adding river temperatures to the runoff inputted into the model.

3.6.1 Air-Sea Forcing

The same MHW analysis performed on model run EPM151 is applied to EPM111. The details of this experiment can be seen in Table 3.1 as well as Section 3.2. CGRF reforecast data only goes as far back as 2002, so choosing an atmospheric dataset which starts farther back in time— where CORE2-IA starts in 1958— may give a more accurate representation of climatology given the longer spin up time the model has. Shown in Figure 3.19 is the SST anomaly time series for EPM111. The SST baseline was taken as the 30-year climatology from 1980 to 2010, following guidelines proposed by the World Meteorological Organization (WMO) on the calculation of climate normals [50]. Notable years in Figure 3.19 include 1998, 2001, and 2005, with maximum temperature anomalies of 5.4^{o}C, 4.9^{o}C, and 4.2^{o}C, respectively.

What is interesting in EPM111 is the recent cold shift in the last decade or so in the run, shown in Figure 3.19 after 2009. A possible explanation for this would be the switch in atmospheric forcing after 2009. The run was first initialized with CORE2-IA reanalysis data, which started in 1958 and ends in 2009. To continue this experiment on to present day, more recent atmospheric forcing data was needed, but non existed as far back as 1958. Thus NCEP reanalysis 2 (NCEP-R2) [52] was chosen to continue this run. It is possible that this atmospheric forcing dataset has a cold bias— thus a stronger heat loss to the atmosphere— that is different to the CORE2-IA dataset. However, Figure 3.20 shows the monthly surface air temperatures from 2002 to 2009 for CORE2-IA and NCEP-R2 datasets do not have significant differences. The two datasets are very similar, with a Pearson's correlation coefficient of r=0.99.

In any case, MHW signatures are captured with the CORE2-IA forcing, notably in the mid to late 1990s. This lines up with observations and stories of told by local Cree and Inuit communities surrounding the Bay of unusual changes in the marine environment during the

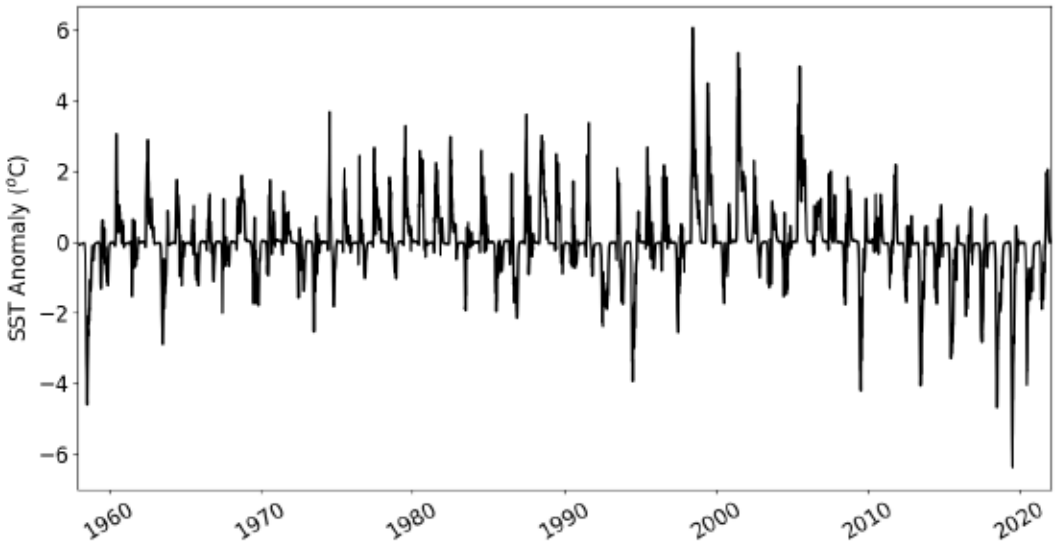

Figure 3.19: EPM111 SST anomaly from 1958-2021 with units of ^{o}C. The SST baseline ranges from 1980-2010. MHW signatures are seen most notably in 1998, 2001, and 2005, with maximum values of 5.4^{o}C, 4.9^{o}C, and 4.2^{o}C, respectively. Pearson's correlation coefficient between the two datasets is r=0.99.

late 90s, including unusual weather and sea ice patterns [2][7].

The calculated horizontal advection (Figure 3.21) and the heat transport at the mouth of James Bay (Figure 3.22) both show seasonal variations, with some years standing out as high heat flux years. For example, the year 2011 shows very strong heat advection and flux into James Bay, which in the same year experiences some of the time series lowest ice concentration in the region (Figure 3.23).

The turbulent sensible, turbulent latent, and the radiative air-sea heat fluxes can be seen in Figures 3.24, 3.25, and 3.26, respectively. Again, an apparent shift— possibly due to the switch to NCEP-R2 atmospheric forcing— can be seen after 2010, especially with the latent heat fluxes (Figure 3.25) and the radiative heat fluxes (Figure 3.26), with higher fluxes going into the ocean, as well as possibly high ocean-to-air fluxes in some years.

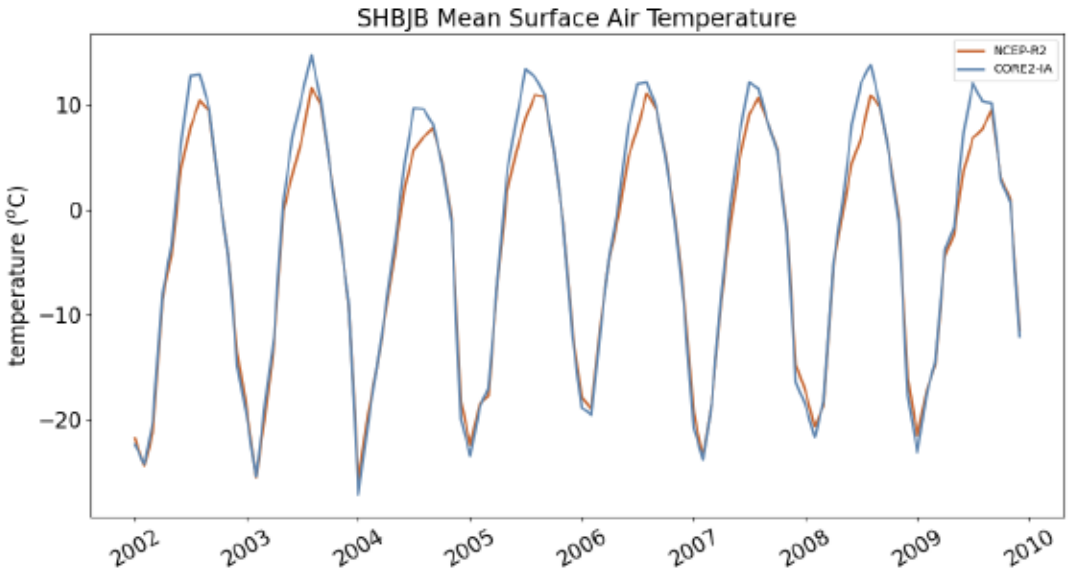

Figure 3.20: SHBJB regional monthly averaged surface air temperatures in ^{o}C from 2002-2009 for CORE2-IA (blue) and NCEP-R2 (orange) reanalysis data.

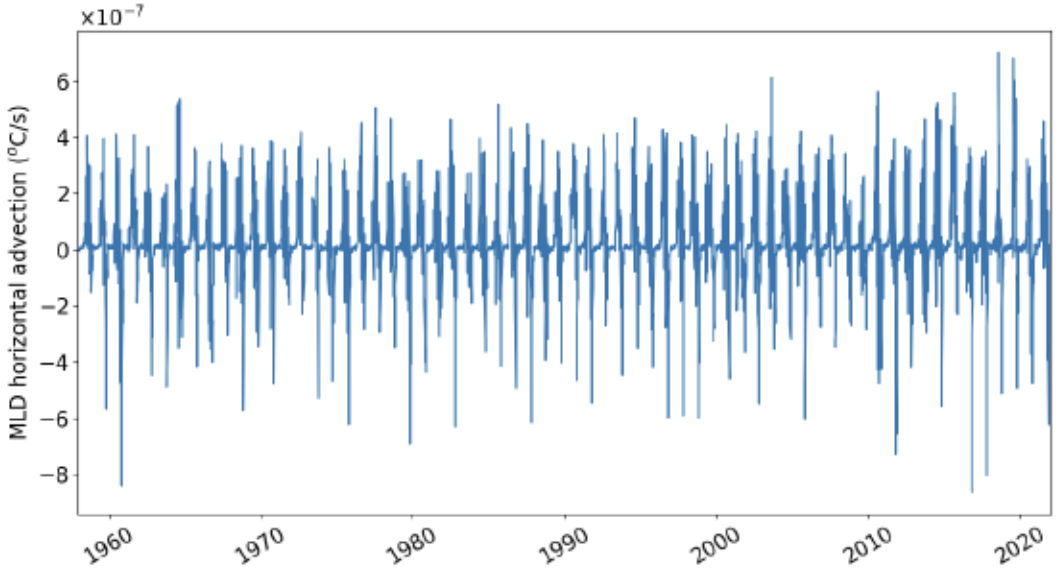

Figure 3.21: EPM111 monthly regional average of horizontal advection (degrees Celsius per second) in SHBJB. The directionality is the same as figure 3.3 for EPM151.

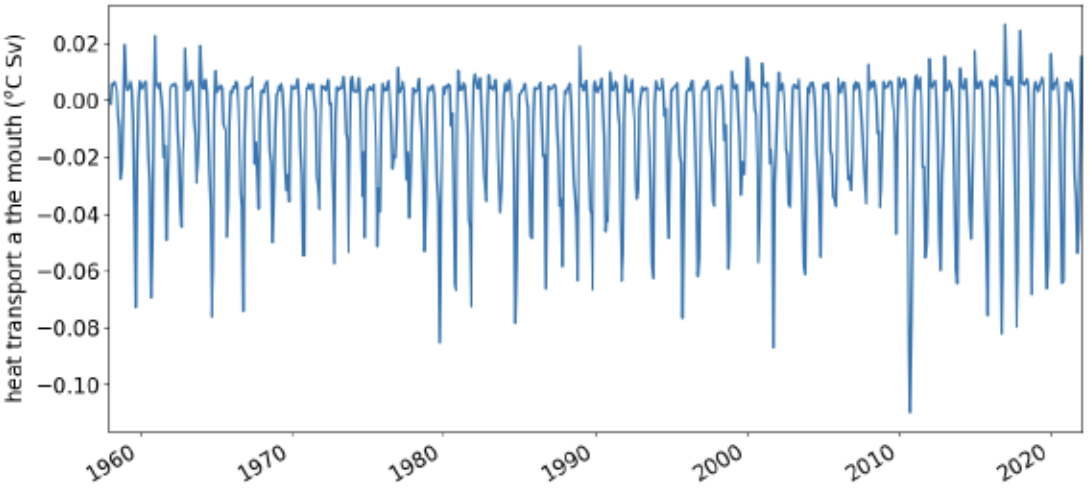

Figure 3.22: Heat transport (degrees Celsius times Sverdrup) at the opening of James Bay for EPM111. Directionality is the same as figure 3.4 for EPM151

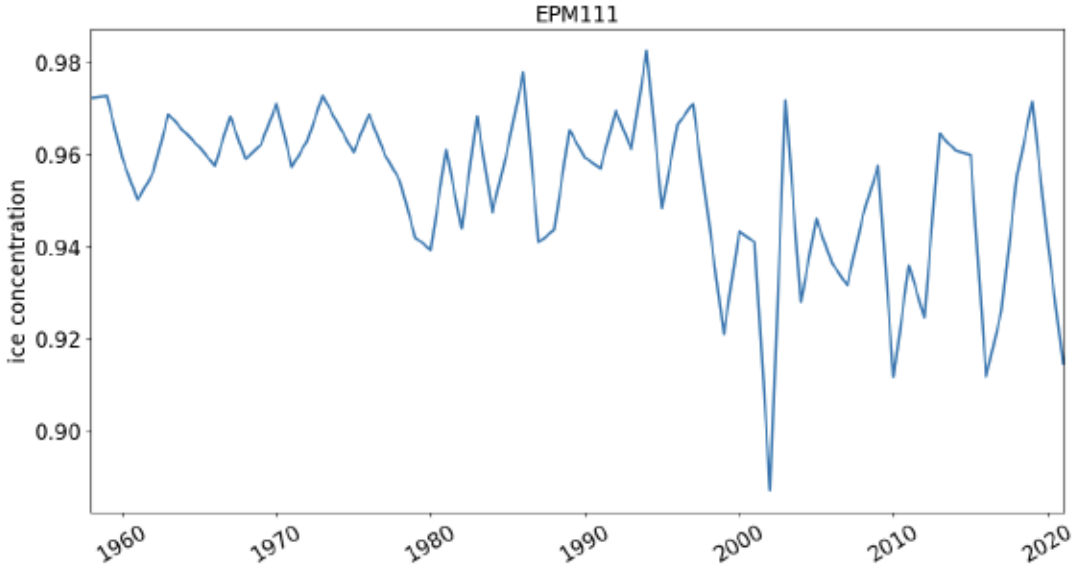

Figure 3.23: EPM111 sea ice concentration— as a fraction of a grid cell— regionally averaged for SHBJB in full ice cover months (January, February, March and April), spanning 1958 to the end of 2021.

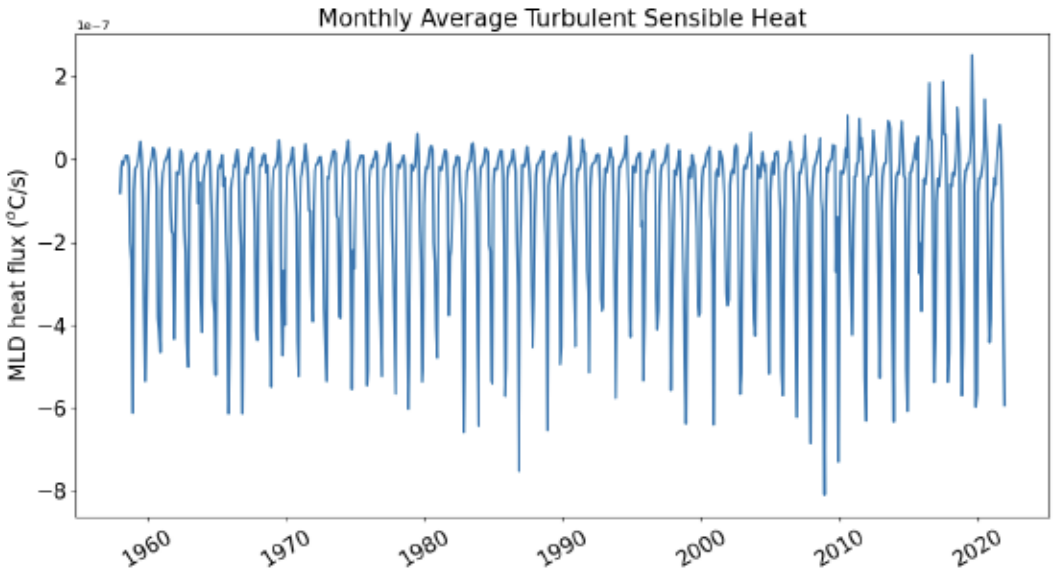

Figure 3.24: EPM111 monthly regional averages of turbulent sensible heat flux with units W/m^2 for years 1958 to 2021.

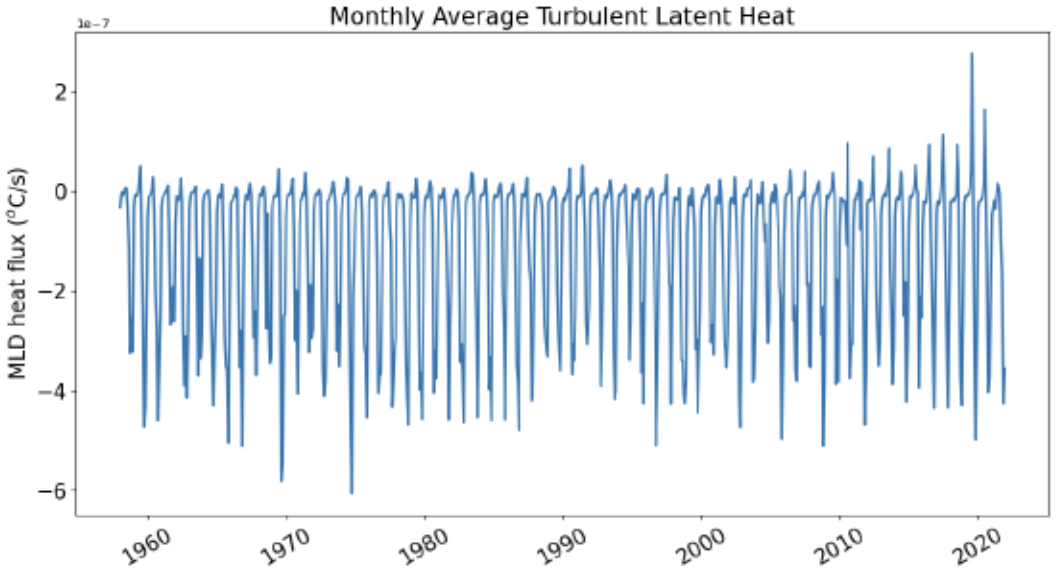

Figure 3.25: EPM111 monthly regional averages of turbulent latent heat flux with units W/m^2 for years 1958 to 2021.

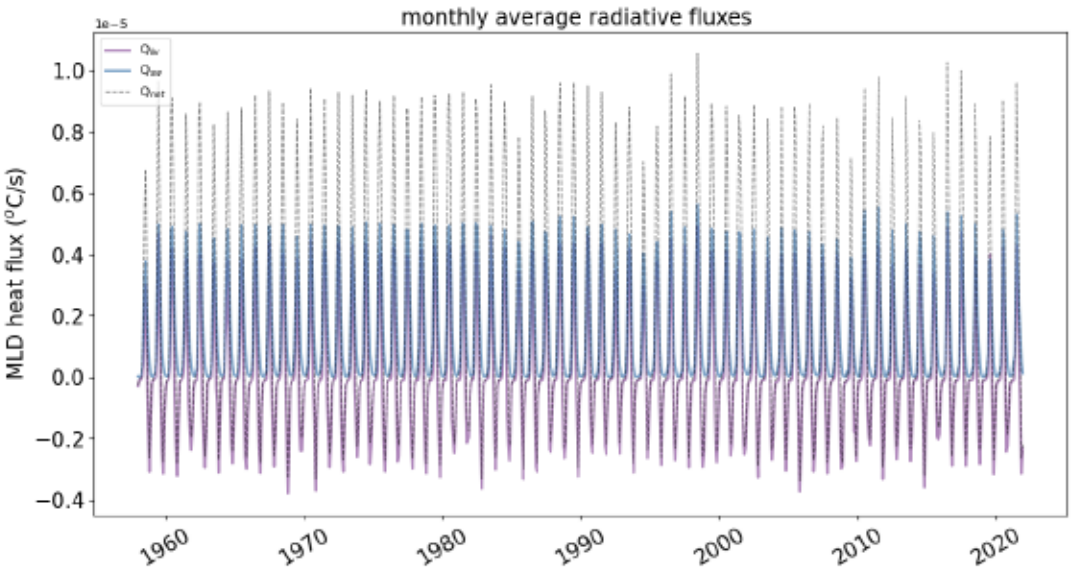

Figure 3.26: EPM111 monthly averages of shortwave, long wave, and net radiative heat flux in W/m^2 for years 1958-2021. The purple solid line is the long wave radiation, the blue solid line is the shortwave radiation, and the dashed black line is the net radiation.

3.6.2 River Heat

The last sensitivity study was done to explore the possible influence of river heat on MHWs in southern Hudson Bay and James Bay. The model run ETW161 (table 3.1) is similar to the base experiment, EPM151, only with updated initial and boundary conditions and different runoff forcing— both using A-HYPE [43] but with ETW161 adding river heat. Figure 3.27 shows the SST anomalies for ETW161. However, looking at figure 3.28, which plots the SST anomalies for experiments with and without river heat, there appears to be almost no discernible difference between the two experiments. What is interesting about contrasting these two experiments against each other is that EPM151 actually has slightly higher SST anomaly peaks during the years with MHW events, which is counter-intuitive to what one might think when adding river heat into the model. However, this may be explained by the fact that ETW161 adds river temperatures to the runoff, which may be colder than what the model ocean temperature is. This is also shown in figure 3.29, which is the difference between EPM151 ad ETW161, where there is less than a quarter of degree Celsius variation at any given time. Because the two experiments are so similar, the MHW analysis for ETW161 follows suit to that of EPM151.

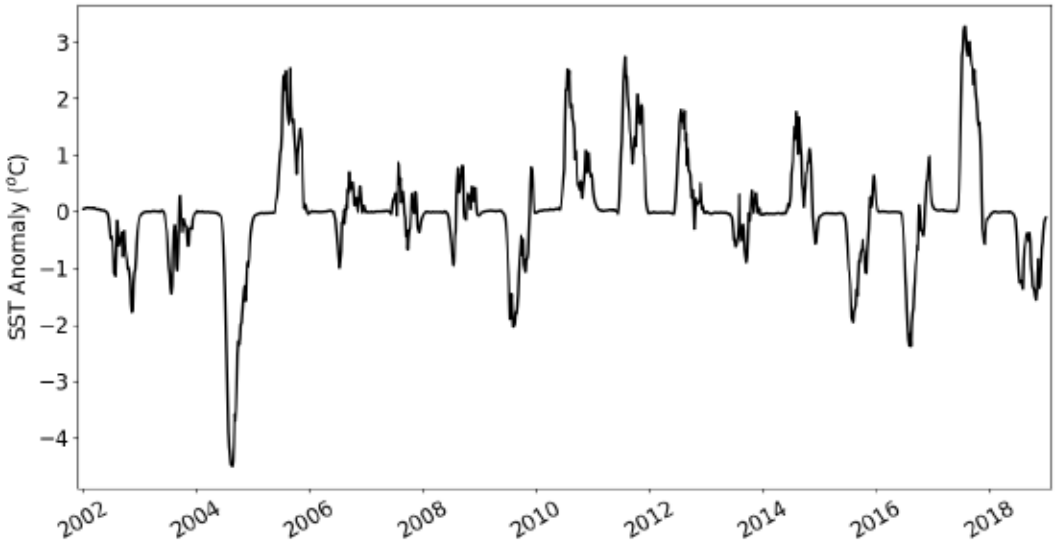

Figure 3.27: ETW161 SST anomaly in degrees Celsius from 2002-2018. MHW signatures are seen in years 2005, 2011, and 2017, with values above 2.5 degrees Celsius for the first two listed years, and over 3 degrees Celsius for 2017.

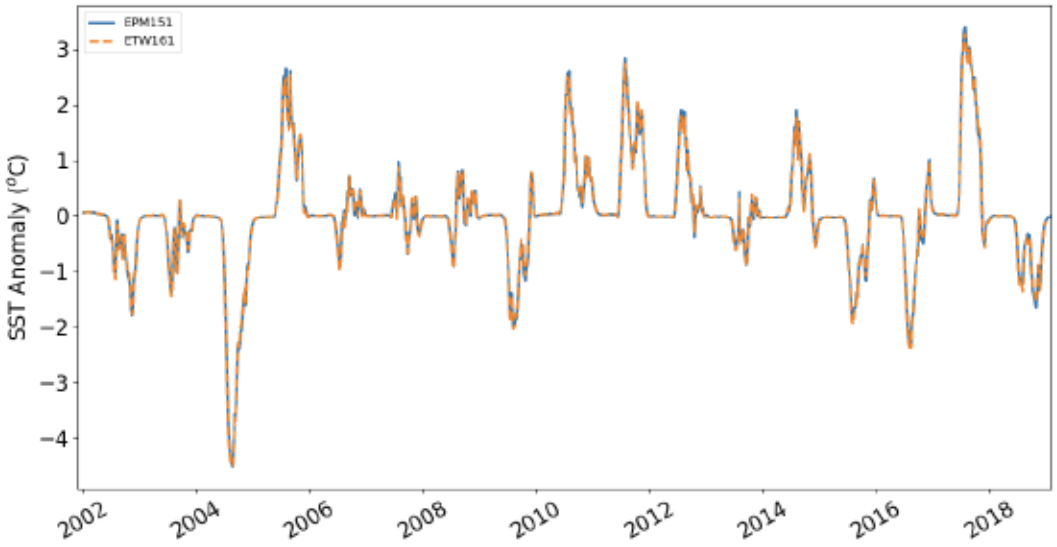

Figure 3.28: EPM151 (solid blue) and ETW161 (dashed orange) SST anomalies in ^{o}C contrasted together.

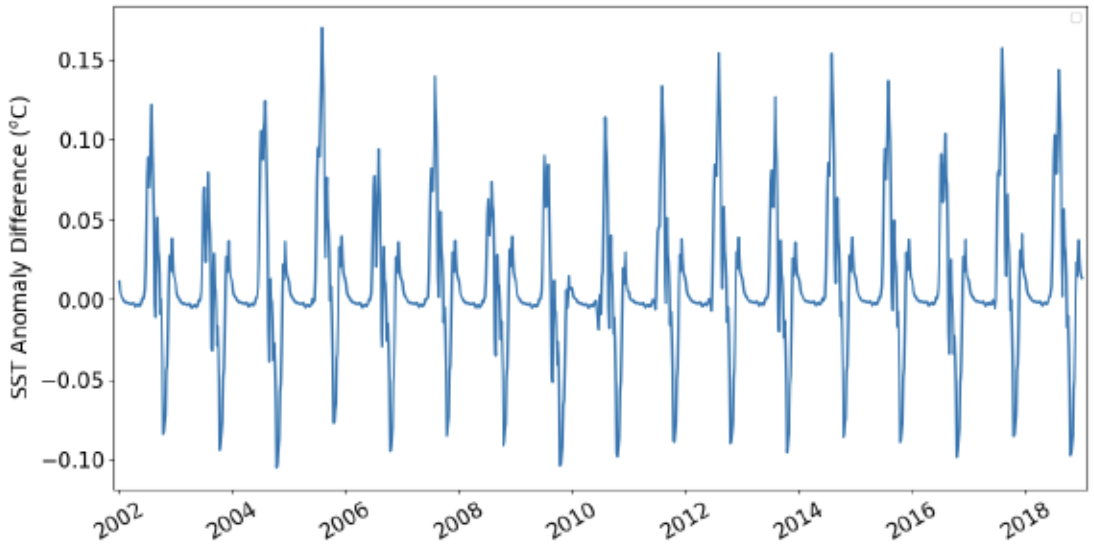

Figure 3.29: The SST anomaly difference between EPM151 and ETW161 in °C. The largest variations between the two experiments range only about 0.25°C.

3.7 Summary

This chapter focused on the main results from the MHW analysis in Southern Hudson Bay and James Bay. This included calculating each term of equation 3.1, giving the horizontal advection and the air-sea heat fluxes. When analysing the MHW drivers for model run EPM151, the main driver appeared to be the radiative fluxes, which onset the MHW event soon after ice cover melted in the region. Horizontal advection of heat and the turbulent heat fluxes also appeared to contribute to MHW events, but more so to prolong them later in the year. Finally, sensitivity studies were performed to see the how atmospheric forcing and river heat influenced MHWs in SHBJB. It was found that the atmospheric forcing can certainly change the years in which MHWs occur and to what intensity, but also shows model bias can occur. Adding river heat shows a null result, at least for this region of the Arctic, where there appears to be no discernible difference in SST anomalies between the two experiments.

Chapter 4

Conclusions

Marine heatwaves are becoming increasingly common in our world today. Arctic Amplification [15] explains why Northern regions are experiencing rapidly changing climates, including more sea ice loss and warmer oceans. In the future, we can expect to see more frequent and intense MHW events in the North, including Hudson Bay and James Bay [18]. This thesis explored and elucidated the processes that drive MHW events in southern Hudson Bay and James Bay using a numerical ocean model. Below are the key findings.

4.1 Key Findings

4.1.1 Radiative heat fluxes are a primary driver for high SST anomaly years, with advection being a secondary driver to prolong events

The initial MHW analysis for the whole time series pointed out two key years with the highest SST anomalies in the series— 2005 and 2017. Case studies of these two events shows the SST

anomaly with the timing of onset and decay of the MHW event, lasting almost the entire ice-free season. Calculating the horizontal advection and each term of the air-sea heat flux (see equation 3.1) shows that in both 2005 and 2017, a spike in the radiative air-sea heat flux lines up with the onset of the MHW right after the ice cover begins to melt. As well, in both cases, the horizontal advection ramps up near the end of the year towards winter, causing either a second MHW event, as in 2005, or prolongs the MHW, as seen in 2017.

4.1.2 Longer atmospheric forcing experiments capture MHW events reported by Indigenous communities, but have unexplained cold bias in recent years

When analyzing the sensitivity experiment with different and longer atmospheric forcing, very high SST anomalies and MHW events in the late 1990s line up with observations from local Cree and Inuit communities who reported changes in the marine environment [7]. These changes included warmer and shorter winters— conducive to more intense MHWs— and unusual ice conditions.

4.1.3 Added river heat not significant in SHBJB region for MHW events

The Hudson Bay Complex serves as one of the largest ocean drainage basins for freshwater in Canada [3]. Currently, many ocean models do not include river temperatures with the provided runoff, despite it possibly playing a role in ocean warming as river temperatures increase with climate change [53]. Despite this, the sensitivity experiment including river heat did not change significantly from the baseline model run with no added river heat in the SHBJB region. In some years, adding river temperatures slightly cooled the SST in the

region. Therefore, with the current data on river temperatures for the Hudson Bay Complex, adding this to the runoff does not affect MHWs in SHBJB.

4.2 Limitations and Future Work

Limitations to this work include the short integration time for the baseline experiment, EPM151, with a time period of 21 years. This does not capture a standard 30-year climatology, as recommended by the World Meteorological Organization (WMO) on the calculation of climate normals [50] and following example from organizations like the International Panel on Climate Change (IPCC). As such, SST anomalies may differ slightly having a shorter climatology period. The observations in the late 1990s by Indigenous communities surrounding the Bay which report the "start" of extreme climatic changes in the region are also missed by this shorter time integration, and thus cannot be compared with the longer integration with atmospheric forcing which includes drastic SST anomalies and MHW events.

Another limitation of this work is the 5-day average of all model output in ANHA4 experiments. This slightly changed the definition of a MHW event when dealing with the model, as any 5-day average output over the 90th percentile threshold was considered a MHW event. This varies slightly from the definition provided by Hobday et al. [19][20], and also smooths out any daily variability that may actually be under the MHW threshold and thus fall out of the definition of a MHW in which the typical definition is that the above threshold temperature must last for at least 5 days.

Future work following this thesis can include providing the same MHW analysis for future climate projections. A comparison of projections can be done as well, with one analysis focusing on the older model projection done for the BAYSYS project, which spans the period 1980-2070, and one analysis focusing on a newer model projection with updated atmospheric forcing taken from the newest CMIP6 climate projections. Other future work may include

performing MHW analysis on higher resolution model configurations—like ANHA12— or perhaps a higher resolution nest for the Hudson Bay and James Bay region.

Bibliography

[1] Nunavut Cambridge Bay. "Elder's Conference on Climate Change". In: (2001).

[2] ZA Kuzyk and LM Candlish. "From science to policy in the greater Hudson Bay marine region: An integrated regional impact study (IRIS) of climate change and modernization". In: *ArcticNet, Québec City* (2019), p. 424.

[3] Environment Canada and Climate Change. *Government of Canada*. Nov. 2017. URL: https://www.canada.ca/en/environment-climate-change/services/freshwater-quality-monitoring/hudson-bay-watershed.html.

[4] RG Ingram and S Prinsenberg. "Coastal oceanography of Hudson Bay and surrounding eastern Canadian Arctic waters". In: *The sea* 11.29 (1998), pp. 835–859.

[5] Simon J Prinsenberg. *Analytical study of the circulation of James Bay*. Fisheries and Environment Canada, 1978.

[6] Ran Tao and Paul G Myers. "Modelling the advection of pollutants in the Hudson Bay complex". In: *Journal of Marine Systems* 214 (2021), p. 103474.

[7] Miriam Anne McDonald, Lucassie Arragutainaq, and Zacharassie Novalinga. "Voices from the Bay: Traditional ecological knowledge of Inuit and Cree in the Hudson Bay bioregion". In: *(No Title)* (1997).

[8] Natasha A Ridenour et al. "Hudson Strait inflow: Structure and variability". In: *Journal of Geophysical Research: Oceans* 126.9 (2021), e2020JC017089.

[9] Igor A Shiklomanov and Alexander I Shiklomanov. "Climatic change and the dynamics of river runoff into the Arctic Ocean". In: *Water Resources* 30 (2003), pp. 593–601.

[10] Natasha A Ridenour et al. "Revisiting the circulation of Hudson Bay: Evidence for a seasonal pattern". In: *Geophysical Research Letters* 46.7 (2019), pp. 3891–3899.

[11] CD Smith et al. "CanCoast: A national-scale framework for characterizing Canada's marine coasts". In: *11th International Symposium for GIS and Computer Cartography for Coastal Zone Management*. 2013.

[12] A-M Hayden et al. "Multi-Century Impacts of Ice Sheet Retreat on Sea Level and Ocean Tides in Hudson Bay". In: *Journal of Geophysical Research: Oceans* 125.11 (2020), e2019JC015104.

[13] Peter S Galbraith and Pierre Larouche. "Reprint of "Sea-surface temperature in Hudson Bay and Hudson Strait in relation to air temperature and ice cover breakup, 1985–2009"". In: *Journal of Marine Systems* 88.3 (2011), pp. 463–475.

[14] Jennifer V Lukovich et al. "Simulated impacts of relative climate change and river discharge regulation on sea ice and oceanographic conditions in the Hudson Bay Complex". In: *Elem Sci Anth* 9.1 (2021), p. 00127.

[15] Roman V Bekryaev, Igor V Polyakov, and Vladimir A Alexeev. "Role of polar amplification in long-term surface air temperature variations and modern Arctic warming". In: *Journal of Climate* 23.14 (2010), pp. 3888–3906.

[16] Mika Rantanen et al. "The Arctic has warmed nearly four times faster than the globe since 1979". In: *Communications Earth & Environment* 3.1 (2022), p. 168.

[17] Walter N Meier and Julienne Stroeve. "An updated assessment of the changing Arctic sea ice cover". In: *Oceanography* 35.3/4 (2022), pp. 10–19.

[18] Benjamin Richaud et al. "Drivers of marine heatwaves in the Arctic Ocean". In: *Journal of Geophysical Research: Oceans* 129.2 (2024), e2023JC020324.

[19] Alistair J Hobday et al. "A hierarchical approach to defining marine heatwaves". In: *Progress in oceanography* 141 (2016), pp. 227–238.

[20] Eric CJ Oliver et al. "Marine heatwaves". In: *Annual review of marine science* 13 (2021), pp. 313–342.

[21] John R Moisan and Pearn P Niiler. "The seasonal heat budget of the North Pacific: Net heat flux and heat storage rates (1950–1990)". In: *Journal of Physical Oceanography* 28.3 (1998), pp. 401–421.

[22] Ce Bian et al. "Oceanic mesoscale eddies as crucial drivers of global marine heatwaves". In: *Nature communications* 14.1 (2023), p. 2970.

[23] Fernando P Lima and David S Wethey. "Three decades of high-resolution coastal sea surface temperatures reveal more than warming". In: *Nature communications* 3.1 (2012), p. 704.

[24] Eric CJ Oliver. "Mean warming not variability drives marine heatwave trends". In: *Climate Dynamics* 53.3 (2019), pp. 1653–1659.

[25] Gurvan Madec et al. "Ocean general circulation model reference manual". In: *Note du Pôle de modélisation* (1997).

[26] Martin Vancoppenolle et al. "The Louvain-la-Neuve sea ice model". In: *Notes du pole de modélisation, Institut Pierre-Simon Laplace (IPSL), Paris, France* 31 (2012).

[27] JL Bamber et al. "Land ice freshwater budget of the Arctic and North Atlantic Oceans: 1. Data, methods, and results". In: *Journal of Geophysical Research: Oceans* 123.3 (2018), pp. 1827–1837.

[28] Fedor Mesinger and Akio Arakawa. "Numerical methods used in atmospheric models". In: (1976).

[29] Andre J Robert. "The integration of a low order spectral form of the primitive meteorological equations". In: *Journal of the Meteorological Society of Japan. Ser. II* 44.5 (1966), pp. 237–245.

[30] Richard Asselin. "Frequency filter for time integrations". In: *Monthly Weather Review* 100.6 (1972), pp. 487–490.

[31] Gurvan Madec et al. "NEMO ocean engine". In: (2017).

[32] William George Large and Stephen G Yeager. *Diurnal to decadal global forcing for ocean and sea-ice models: The data sets and flux climatologies*. 2004.

[33] Thierry Fichefet and MA Morales Maqueda. "Sensitivity of a global sea ice model to the treatment of ice thermodynamics and dynamics". In: *Journal of Geophysical Research: Oceans* 102.C6 (1997), pp. 12609–12646.

[34] Ralph Timmermann et al. "On the representation of high latitude processes in the ORCA-LIM global coupled sea ice–ocean model". In: *Ocean Modelling* 8.1-2 (2005), pp. 175–201.

[35] Sylvain Bouillon et al. "An elastic–viscous–plastic sea ice model formulated on Arakawa B and C grids". In: *Ocean Modelling* 27.3-4 (2009), pp. 174–184.

[36] WD Hibler III. "A dynamic thermodynamic sea ice model". In: *Journal of physical oceanography* 9.4 (1979), pp. 815–846.

[37] Elizabeth C Hunke and John K Dukowicz. "The elastic–viscous–plastic sea ice dynamics model in general orthogonal curvilinear coordinates on a sphere—Incorporation of metric terms". In: *Monthly Weather Review* 130.7 (2002), pp. 1848–1865.

[38] Laura C Gillard. "Modelling the Interconnection of the Ocean and the Greenland Ice Sheet". In: (2021).

[39] *Mercator Ocean*. `https://www.mercator-ocean.eu/en/ocean-science/glorys/`. Accessed: 2024-06-10.

[40] Michael Steele, Rebecca Morley, and Wendy Ermold. "PHC: A global ocean hydrography with a high-quality Arctic Ocean". In: *Journal of Climate* 14.9 (2001), pp. 2079–2087.

[41] Seiji Yukimoto et al. "A new global climate model of the Meteorological Research Institute: MRI-CGCM3—Model description and basic performance—". In: *Journal of the Meteorological Society of Japan. Ser. II* 90.0 (2012), pp. 23–64.

[42] A Dai. *Dai and Trenberth Global River Flow and Continental Discharge Dataset [Dataset].* Accessed: 2024-06-10. 2017. DOI: https://doi.org/10.5065/D6V69H1T.

[43] TA Stadnyk et al. *Hydrological modeling of freshwater discharge into Hudson Bay using HYPE. Elem. Sci. Anthr. 8.* 2020.

[44] Christiaan T van Dalum et al. "First results of the polar regional climate model RACMO2. 4". In: *EGUsphere* 2024 (2024), pp. 1–36.

[45] Gregory C Smith et al. "A new atmospheric dataset for forcing ice–ocean models: Evaluation of reforecasts using the Canadian global deterministic prediction system". In: *Quarterly Journal of the Royal Meteorological Society* 140.680 (2014), pp. 881–894.

[46] Tahya WeissGibbons et al. "Increased runoff from Siberian rivers leads to Arctic wide freshening". preprint available at https://essopenarchive.org/users/659901/articles/663686-increased-runoff-from-siberian-rivers-leads-to-arctic-wide-freshening.

[47] *Advanced Microwave Scanning Radiometer 2 (AMSR2).* https://www.earthdata.nasa.gov/learn/find-data/near-real-time/amsr2. Accessed: 2024-07-08.

[48] *Southern Hudson Bay - James Bay CTD Data 2021.* https://canwin-datahub.ad.umanitoba.ca/data/dataset/hudson-bay-james-bay-ctd-2021. Accessed: 2024-07-08.

[49] *Kiel Climate Model System.* https://www.geomar.de/kcms. Accessed: 2024-07-12.

[50] *WMO guidelines on the calculation of climate normals.* Doc. WMO-No. 1203, WMO, Geneva. 2017.

[51] Alistair J Hobday et al. "Categorizing and naming marine heatwaves". In: *Oceanography* 31.2 (2018), pp. 162–173.

[52] *NCEP/DOE Reanalysis II.* ttps://psl.noaa.gov/data/gridded/data.ncep.reanalysis2.tml. Accessed: 2024-06-42.

[53] Daqing Yang et al. "Heat flux, water temperature and discharge from 15 northern Canadian rivers draining to Arctic Ocean and Hudson Bay". In: *Global and Planetary Change* 204 (2021), p. 103577.